

**EXPERIMENTAL AND NUMERICAL STUDY ON
COLD-FORMED STEEL BUILT-UP BOX BEAMS
WITH DIFFERENT SECTIONS**

BY

BUNYA CHEA

**A THESIS SUBMITTED IN PARTIAL FULFILLMENT OF THE
REQUIREMENTS FOR THE DEGREE OF MASTER OF SCIENCE
(ENGINEERING AND TECHNOLOGY)
SIRINDHORN INTERNATIONAL INSTITUTE OF TECHNOLOGY
THAMMASAT UNIVERSITY
ACADEMIC YEAR 2016**

**EXPERIMENTAL AND NUMERICAL STUDY ON
COLD-FORMED STEEL BUILT-UP BOX BEAMS
WITH DIFFERENT SECTIONS**

BY

BUNYA CHEA

**A THESIS SUBMITTED IN PARTIAL FULFILLMENT OF THE
REQUIREMENTS FOR THE DEGREE OF MASTER OF SCIENCE
(ENGINEERING AND TECHNOLOGY)
SIRINDHORN INTERNATIONAL INSTITUTE OF TECHNOLOGY
THAMMASAT UNIVERSITY
ACADEMIC YEAR 2016**

EXPERIMENTAL AND NUMERICAL STUDY ON COLD-FORMED
STEEL BUILT-UP BOX BEAMS WITH DIFFERENT SECTIONS

A Thesis Presented

By

BUNYA CHEA

Submitted to

Sirindhorn International Institute of Technology

Thammasat University

In partial fulfillment of the requirements for the degree of
MASTER OF SCIENCE (ENGINEERING AND TECHNOLOGY)

Approved as to style and content by

Advisor and Chairperson of Thesis Committee



(Assoc. Prof. Dr. Taweep Chaisomphob)

Committee Member and

Chairperson of Examination Committee



(Dr. Pakawat Sancharoen)

Committee Member



(Assoc. Prof. Dr. Piya Chotickai)

JUNE 2017

Abstract

EXPERIMENTAL AND NUMERICAL STUDY ON COLD-FORMED STEEL BUILT-UP BOX BEAMS WITH DIFFERENT SECTIONS

by

BUNYA CHEA

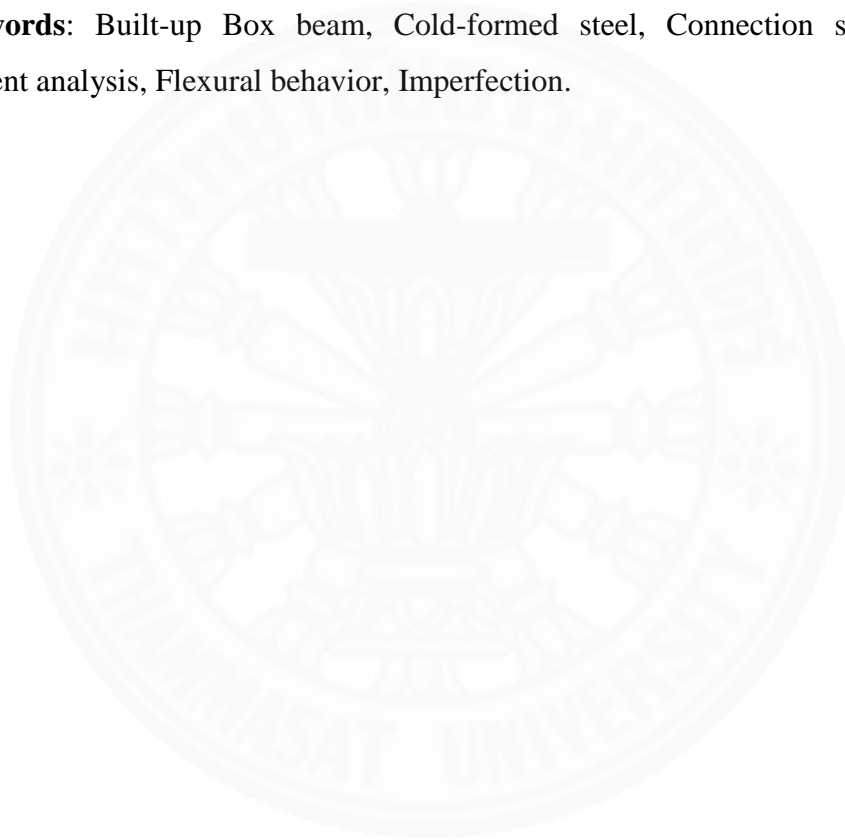
Bachelor of Civil Engineering, Institute of Technology of Cambodia, 2015

Master of Science (Engineering and Technology), Sirindhorn International Institute of Technology, 2017

Currently, the use of cold-formed steel member has been more popular even in developing country. It has been used for small and medium structures, especially roof structures. The built-up closed section is the most desirable section, since the torsional resistance of the built-up closed section is excellent in comparison of that of the single open section. Built-up box beam was considered in this research. The connection with self-drilling screws was chosen because it is more advantageous than the welding connection, in which the coating of cold-formed steel section may be destroyed by welding process. For the design specification, such as AISI 2012, the design method of the built-up is not clearly written. In this study, experimental study was focused to understand the flexural behavior of cold-formed steel built-up box beams composed of two face-to-face C sections. Built-up box beams made of five different C sections: C10012, C10015, C10019, C15012, and C15015 were tested. In addition, four different connection spacings equal to $L/2$, $L/3$, $L/4$, and $L/6$ (where L is representative span length) were chosen. Therefore, in the present test of the built-up box beams, there are 20 beam specimens. In the numerical study, a suitable finite element model was developed in order to compare with the experimental results. Initial geometry imperfection and geometrical/material nonlinearity were considered in the analysis. Both experimental results and those of finite element analysis showed

that the capacity of the beam got higher when thickness of the section was increased and the connection spacing reduced. From the experimental results, the failure modes with connection spacing $L/4$ or smaller were local buckling, and the failure modes with connection spacing larger than $L/4$ were mixed modes of local buckling and distortional buckling, or lateral torsional buckling. The results from finite element analysis reasonably agreed with experimental results. Thus, the proposed computational modeling can be used to predict the behavior of the built-up box beam.

Keywords: Built-up Box beam, Cold-formed steel, Connection spacing, Finite element analysis, Flexural behavior, Imperfection.



Acknowledgements

First and foremost, I am sincerely appreciative and thankful to my advisor Assoc. Prof. Dr. Taweep Chaisomphob for his expert guidance and valuable suggestions for the whole of master degree program. His constructive assistance and teaching made me try to study harder.

I grateful acknowledge my thesis committee members Dr. Pakawat Sancharoen and Assoc. Prof. Dr. Piya Chotickai, who gave me useful comments and suggestions on my thesis to improve it better. I would also like to acknowledge Mr. Wasan Patwichaichote and Mr. Ha Thanh Tran, PhD students at Sirindhorn International Institute of Technology, Thammasat University, for their suggestion on the part of discussion on the test and numerical results.

I would like to deeply thank AUN-SEED/Net and Sirindhorn International Institute of Technology, Thammasat University for their scholarship. I also thank the School of Civil Engineering for their support and assistance during my master program and NS BlueScope Lysaght (ThaiLand) Limited for their material support. I would like to appreciate laboratory of the Chulachomklao Royal Military Academy (CRMA) for providing facilities and thank the technicians at there for their support.

Through the academic agreement between SIIT, Thammasat University and Faculty of Engineering, Kyushu Institute of Technology, this study has been partially supported by the two academic bodies, especially for the ABAQUS program.

Finally, I would also like to specially thank my parents, my relatives, seniors, juniors, and all of my friends for their endless support, and encouragement throughout the duration of my master degree.

Table of Contents

Chapter	Title	Page
	Signature page	i
	Abstract	ii
	Acknowledgements	iv
	Table of Contents	v
	List of Tables	vii
	List of Figures	viii
1	Introduction	1
	1.1 General	1
	1.2 Statement of problem	3
	1.3 Purpose and scope of study	5
2	Literature review	6
	2.1 General	6
	2.2 Design specification	6
	2.2.1 Effective width method	6
	2.2.2 Direct strength method	6
	2.3 Failure mode of C section	8
	2.3.1 Local buckling	8
	2.3.2 Distortional buckling	8
	2.3.3 Lateral torsional buckling	9
	2.4 Past experimental and numerical investigation on the built-up cold-formed steel beams	10
	2.5 Computational modeling study	24
3	Experimental study	27

3.1	Experimental method	27
3.1.1	Material and specimen properties	27
3.1.2	Test set-up	30
3.1.3	Test procedure	33
3.2	Experimental results and discussion	34
3.2.1	Influence of web height and flange width to thickness ratio on load capacity	35
3.2.2	Influence of the thickness on load capacity	36
3.2.3	Influence of connector spacing on load capacity	37
3.2.4	Load-deflection curve	39
3.2.5	Load-strain curve	41
3.2.6	Failure mode	43
4	Numerical study	49
4.1	Numerical method	49
4.1.1	Element type	49
4.1.2	Material properties	50
4.1.3	Fastener and contact condition	50
4.1.4	Boundary and loading	54
4.1.5	Finite element mesh	54
4.1.6	Analytic procedure	55
4.2	Numerical results and discussion	56
4.2.1	Key factors improving load capacity of the beam	58
4.2.2	Comparison of load-vertical deflection curve between experimental and FEA results	59
4.2.3	Comparison of failure mode from experiment and FEA	63
5	Conclusion and Recommendation	68
	References	70

List of Tables

Tables	Page
3.1 Dimension of C section	27
3.2 Details of specimen	29
3.3 Test results	35
4.1 FEA results and test results	57



List of Figures

Figures	Page
1.1 Method of forming of cold-formed steel sections: (a): Cold rolling machine, (b): Press brake operation, (c): Bending brake operation	1
1.2 Steel coil	2
1.3 Type of cold-formed steel sections (Design of Cold-formed steel structures by Dan Dubina)	2
1.4 Beam support the load	3
1.5 C section of the beam	3
1.6 Torsion of closed and open thin-walled section	4
1.7 Built-up C face to face	4
1.8 Connection types for cold-formed steel	4
1.9 Screw connection with stiffening plate used in this thesis (80x80x2mm)	5
2.1 Local buckling	8
2.2 Flange distortional buckling	8
2.3 Lateral distortional buckling	8
2.4 Lateral torsional buckling	9
2.5 Buckling modes of Lipped channel beams in bending (Hancock, 2003)	9
2.6 (a) Schematic diagram of four-point bending test, (b) Cross section (Tran et al., 2015)	10
2.7 Overall view of bending test (Tran et al., 2015)	11
2.8 Built-up box test assembly (Xu et al., 2009)	12
2.9 Finite element model (Xu et al., 2009)	13
2.10 Local buckling of compressive flange of track section in FE analysis and the test (Xu et al., 2009)	14
2.11 The cross-sections of the tested beams (Laim et al., 2013)	17
2.12 Schematic view of the experimental set-up for bending tests (Laim et al., 2013)	17

2.13 Numerical model used in the finite element analysis: (a) perspective and (b) cross-sectional view (Laim et al., 2013)	18
2.14 FEA (a) and experimental (b) failure modes for the box beam (Laim et al., 2013)	19
2.15 FEM model for beam with connection spacing $L/2$ (Tran et al., 2016)	19
2.16 Main failure mode comparison between test and FEM test results for C15019 beam with different connection spacing 1750mm (Tran et al., 2016)	20
2.17 Lateral torsional buckling of specimen B4 (Manikandan et al., 2016)	21
2.18 Typical failure modes: (a) CU140x50x12x1.2-X-2, (b) CU140x50x12x1.2-Y-1 (Li et al., 2016)	22
2.19 A comparison between experimental and numerical (a) local and (b) distortional buckling failure mode subjected to pure bending test (Tahir et al. 2015)	23
2.20 Element choice (linear and quadratic) and mesh densities for parametric study (Schafer et al., 2010)	24
2.21 Membrane plastic strain, during collapse (at an end shortening 4mm) for different elements and mesh densities (Schafer et al., 2010)	25
3.1 Stress-strain relationship of material of thickness 1.2mm	28
3.2 Stiffening plate (80x80x2mm) with 4 screws	28
3.3 Cee cross section	29
3.4 Built-up box C section: (a) BBC-15012, (b) BBC-15015	30
3.5 Built-up box C section: (a) BBC-10012, (b) BBC-10015, (c) BBC-10019	30
3.6 Test setting up for BBC-15012 connection spacing 1750mm	31
3.7 Support system	31
3.8 Checking the centerlines	32
3.9 Test set-up for four-point bending test	32
3.10 Strain and vertical deflection measurement	33
3.11 (a): Data logger, (b): hydraulic pump	33
3.12 Strain gauge and LVDT locations at the section A-A in the tests	34
3.13 Max load-web height to thickness ratio curve for thickness 1.2, 1.5 and 1.9 mm with $L/6$, $L/4$, $L/3$, and $L/2$	36
3.14 Max load-flange width to thickness ratio curve for thickness 1.2, 1.5 and 1.9 mm with $L/6$, $L/4$, $L/3$, and $L/2$	36

3.15 Max load associated with variation of thickness 1.2, 1.5 and 1.9 mm for L/6, L/4, L/3, and L/2. (BBC-100)	37
3.16 Max load associated with variation of thickness 1.2, and 1.5 mm for L/6, L/4, L/3, and L/2. (BBC-150)	37
3.17 Max load associated with variation of connection spacing L/6, L/4, L/3, and L/2 for t=1.2, 1.5, and 1.9mm. (BBC-100)	38
3.18 Max load associated with variation of connection spacing L/6, L/4, L/3, and L/2 for t=1.2, and 1.5 mm (BBC-150)	38
3.19 Comparison between load-vertical deflection curve of LVDT1 and LVDT2: (a) BBC-10015L/6, and (b) BBC-15012L/2	39
3.20 Load-vertical deflection curve with connection spacing L/2, L/3, L/4, and L/6: (a) BBC-10012, (b) BBC-10015, (c) BBC-10019, (d) BBC-15012, and (e) BBC-15015	40
3.21 Load-lateral deflection curve of BBC-15015 with connection spacing L/2, L/3, L/4, and L/6	41
3.22 Load-strain curve of section A-A 100 mm away from mid-span: (a) BBC-10019L/2, and (b) BBC-15012L/4	41
3.23 Load-strain curve with connection spacing L/2, L/3, L/4, and L/6: (a) BBC-10012, (b) BBC-10015, (c) BBC-10019, (d) BBC-15012, (e) BBC-15015	42
3.24 Failure mode of BBC-10012	43
3.25 Failure mode of BBC-10015	44
3.26 Failure mode of BBC-10019	45
3.27 Failure mode of BBC-15012	46
3.28 Failure mode of BBC-15015	47
4.1 The meaning of index representation: (a): Shell element, (b): Solid element	50
4.2 Screw connection modeling	51
4.3 Surface to surface contact of lip with lip	52
4.4 Surface to surface of load bearing plate with C sections	53
4.5 Tie contact between C sections and the support bearing plate	53
4.6 Support conditions and loading modeling	54
4.7 Mesh of corner curves and lips of C sections	55

4.8 The comparison of the shape between section imperfection and no imperfection for BBC-10012L/2	56
4.9 Max load-web height to thickness ratio curve of experiment and FEA with L/6, L/4, L/3, and L/2	58
4.10 Max load-flange width to thickness ratio curve of experiment and FEA with L/6, L/4, L/3, and L/2	58
4.11 Comparison of load-vertical deflection curve between experimental and FEA results: (a): BBC-10012L/6; (b): BBC-10012L/4; (c): BBC-10012L/3; (d): BBC-10012L/2	59
4.12 Comparison of load-vertical deflection curve between experimental and FEA results: (a): BBC-10015L/6; (b): BBC-10015L/4; (c): BBC-10015L/3; (d): BBC-10015L/2	60
4.13 Comparison of load-vertical deflection curve between experimental and FEA results: (a): BBC-10019L/6; (b): BBC-10019L/4; (c): BBC-10019L/3; (d): BBC-10019L/2	61
4.14 Comparison of load-vertical deflection curve between experimental and FEA results: (a): BBC-15012L/6; (b): BBC-15012L/4; (c): BBC-15012L/3; (d): BBC-15012L/2	62
4.15 Comparison of load-vertical deflection curve between experimental and FEA results: (a): BBC-15015L/6; (b): BBC-15015L/4; (c): BBC-15015L/3; (d): BBC-15015L/2	63
4.16 Comparison of failure mode from experiment and finite element analysis: (a): BBC-10012L/6, (b) BBC-10012L/2	64
4.17 Comparison of failure mode from experiment and finite element analysis: (a): BBC-10015L/6, (b) BBC-10015L/4, (c) BBC-10015L/3	65
4.18 Comparison of failure mode from experiment and finite element analysis: (a): BBC-10019L/6	66
4.19 Comparison of failure mode from experiment and finite element analysis: (a): BBC-15012L/6, (b) BBC-15012L/4	66
4.20 Comparison of failure mode from experiment and finite element analysis: (a): BBC-15015L/6, (b) BBC-15015L/4	67

Chapter 1

Introduction

1.1 General

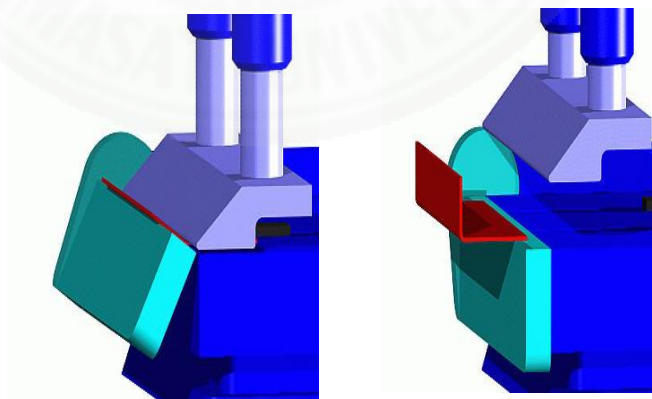
Recently, cold-formed steel has been adopted in the construction of small and medium buildings. It was introduced in United States and Great Britain since 1950s. There are three types of methods of forming of cold-formed steel section, such as cold roll forming, press brake operation, and bending brake operation (Figure 1.1). It is made from steel coil as shown in Figure 1.2.



(a)



(b)



(c)

Figure 1.1 Method of forming of cold-formed steel sections: (a): Cold rolling machine, (b): Press brake operation, (c): Bending brake operation



Figure 1.2 Steel coil

The cold-formed steel thickness varies from 0.4 mm to 6.0 mm. We can divide cold-formed steel section into three types, such as single open sections, built-up open sections, and built-up closed sections (Figure 1.3).

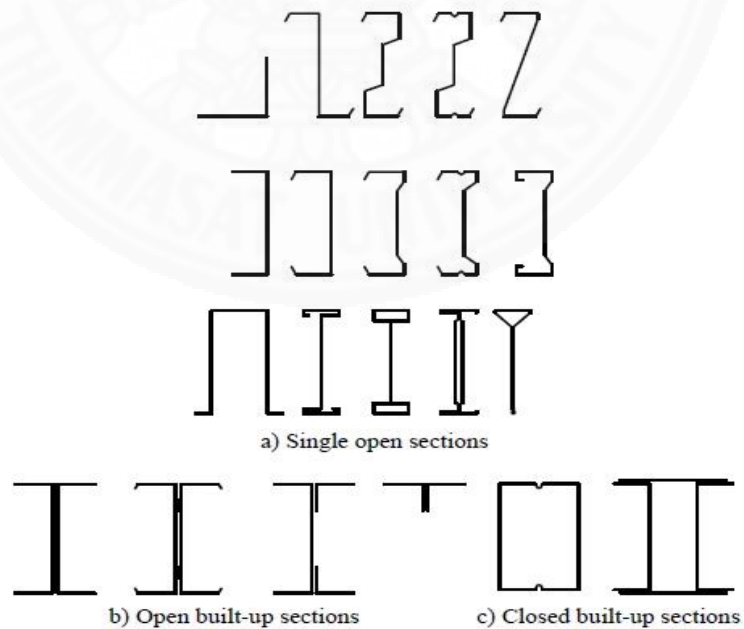


Figure 1.3 Type of cold-formed steel sections (Design of Cold-formed steel structures by Dan Dubina)

It has a lot of advantages because it has light weight and easy to install. It has been applied into several types of structures, for example: metal building construction, wall framing, floor framing, and roof framing. Because of its thin thickness, it was regarded as the thin-walled members.

It did not have any good specifications for design. Because of the increasing of using cold-formed steel in construction, this pushes AISI (American Iron and Steel Institute) to publish the design code for structural cold-formed steel. Researches on cold-formed steel have been continuously conducted, since the behavior of thin-walled members is quite complicated.

1.2 Statement of problem

Among three types of sections described above, the single open section is the easiest one for design and installation. However, in case of higher loads, the built-up section is needed. A single C section steel beam with a simple support is shown in Figure 1.4 & Figure 1.5.

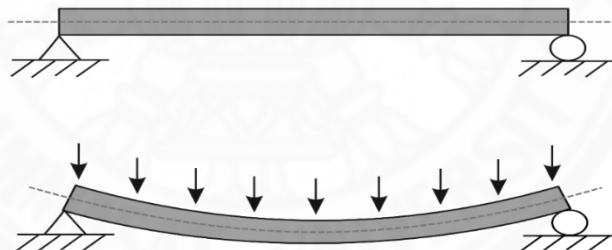


Figure 1.4 Beam support the load

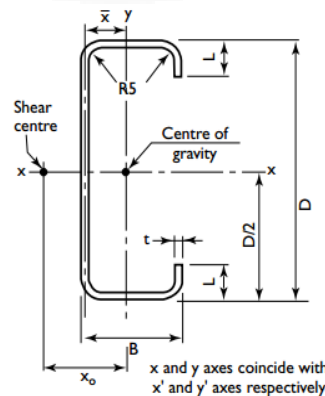


Figure 1.5 C section of the beam

Suppose that the largest available C section be insufficient to support the loads anticipated for certain span. Sometime, the total depth may be so limited that the resisting moments of C sections of specified depth are too small. Built-up girder in this case is box girder C face to face.

Since torsion is one of the key influences on the design of thin-walled steel structures, the built-up box closed section is introduced in the practical design since it has higher torsional strength than the open section (Figure 1.6).



Figure 1.6 Torsion of closed and open thin-walled section

In this study, built-up box shown in Figure 1.7 is considered.



Figure 1.7 Built-up C face to face

There are three common types of cold-formed steel connection as seen in Figure 1.8.



Figure 1.8 Connection types for cold-formed steel

Since, the cold-formed steel thickness is very thin, screw connection is the most suitable connection. In addition, Screw connection is easy to be installed, especially for the cold-formed steel structures.

Figure 1.9 shows the screw connection with stiffening plate for the built-up box beams in the present study.



Figure 1.9 Screw connection with stiffening plate used in this thesis (80x80x2mm)

1.3 Purpose and scope of study

The main purpose of this research is to conduct the experimental study on the flexural behavior of cold-formed steel built-up box beams under four-point loading in order to have the constant bending moment in the middle of the span. The numerical analysis by the finite element program ABAQUS 6.14-1 is performed, and the numerical results are compared with the experimental results.

Sections of the beam specimen are as follows: BBC-10012, BBC-10015, BBC-10019, BBC-15012, and BBC-15015 (BBC- : Built-up Box C-). The connection spacings are varied to be $L/2$, $L/3$, $L/4$, and $L/6$, where L is the representative span length (3.5 m).

Chapter 2

Literature review

2.1 General

This chapter describes about the review of literatures on cold-formed steel, the design formula, experiments on built-up beams, and computational modeling.

2.2 Design specification

There are no specific guideline for calculating the flexural strength of built-up box section. The current design code AISI 2012 provides two design methods to calculate flexural strength moment capacity of single members.

2.2.1 Effective width method

AISI, North American Specification for Design of Cold-Formed Steel Structural Members, 2012 edition, provides the formula to calculate the section strength of flexural single members. The nominal section strength for the initiation of yielding is calculated by using the following equation:

$$M_n = M_y = S_e F_y \quad (2.1)$$

F_y = design yield stress, and S_e = effective elastic section modulus. Effective elastic section modulus S_e is calculated based on the effective width of individual elements of the section under design yield stress.

In the design of cold-formed steel flexural members, the moment-resisting capacity of the member could be limited by lateral buckling of the beam, particularly when the open section is fabricated from thin material and laterally supported at relatively large intervals. Cold-formed steel beams generally fail due to material yielding, local buckling, distortional buckling, and lateral torsional buckling.

2.2.2 Direct strength method

Based on the AISI, North American Specification for Design of Cold-Formed Steel Structural Members, 2012 edition, nominal flexural strength of cold-formed steel member M_n is equal to $\min(M_{ne}, M_{nl}, \text{ and } M_{nd})$.

- M_{ne} : lateral torsional buckling strength

- For $M_{cre} < 0.56M_y$: $M_{ne} = M_{cre}$ (2.2)

- For $2.78M_y \geq M_{cre} \geq 0.56M_y$: $M_{ne} = \frac{10}{9} M_y \left(1 - \frac{10M_y}{36M_{cre}} \right)$ (2.3)

- For $M_{cre} > 2.78M_y$: $M_{ne} = M_y$ (2.4)

$M_{cre} = S_f f_{cre}$: critical elastic lateral torsional buckling moment

Where, S_f : gross section modulus to the extreme compression fiber

f_{cre} : elastic critical lateral torsional buckling stress. $f_{cre} = F_e$ of main specification section C3.1.2.2.

$M_y = S_f F_y$: Member yield moment

- M_{nl} : Local buckling strength

- For $\lambda_1 = \sqrt{M_{ne} / M_{cr\ell}} \leq 0.776$: $M_{nl} = M_{ne}$ (2.5)

- For $\lambda_1 = \sqrt{M_{ne} / M_{cr\ell}} > 0.776$: $M_{nl} = \left(1 - 0.15 \left(\frac{M_{cr\ell}}{M_{ne}} \right)^{0.4} \right) \left(\frac{M_{cr\ell}}{M_{ne}} \right)^{0.4} M_{ne}$ (2.6)

M_{ne} : Lateral torsional buckling strength

$M_{cr\ell} = S_f f_{cr\ell}$: Critical elastic local buckling moment

Where, $f_{cr\ell} = k \frac{\pi^2 E}{12(1-\mu^2)} \left(\frac{t}{w} \right)^2$: local buckling stress at the extreme

compression fiber, determined in accordance with Section 1.1.2 of Appendix 1: commentary on Direct Strength Method

- M_{nd} : Distortional buckling strength

- For $\lambda_d = \sqrt{M_y / M_{crd}} \leq 0.673$: $M_{nd} = M_y$ (2.7)

- For $\lambda_d = \sqrt{M_y / M_{crd}} > 0.673$: $M_{nd} = \left(1 - 0.22 \left(\frac{M_{crd}}{M_y} \right)^{0.5} \right) \left(\frac{M_{crd}}{M_y} \right)^{0.5} M_y$ (2.8)

$M_y = S_f F_y$: Member yield moment

$M_{nd} = S_f f_{crd}$: Critical elastic distortional buckling moment

Where, f_{crd} : elastic distortional buckling stress, determined in accordance with Section 1.1.2 of Appendix 1: commentary on Direct Strength Method

For more details, it is available on the AISI, North American Specification for Design of Cold-Formed Steel Structural Members, 2012 edition.

2.3 Failure mode of C section

2.3.1 Local buckling

The buckling each of the plate which is subjected to compression is called local buckling. The local buckling of C section has shown in Figure 2.1.

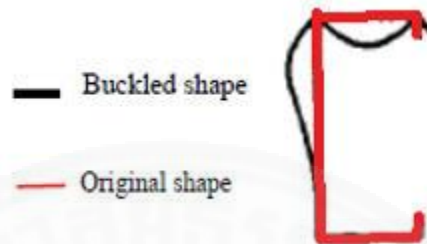


Figure 2.1 Local buckling

2.3.2 Distortional buckling

Cold-formed steel could meet a kind of buckling mode, called distortional buckling. In the flange distortional buckling, the flange and the lip rotate, but the joints between flange and web are still at the same position (Figure 2.2).

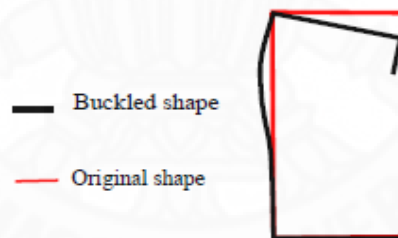


Figure 2.2 Flange distortional buckling

The lateral distortional buckling occurs when the top flange and the lip rotate and the joints between flange and web also move (Figure 2.3).

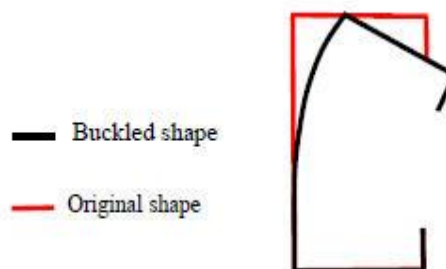


Figure 2.3 Lateral distortional buckling

2.3.3 Lateral torsional buckling

One of the critical failure mode of steel beams is called lateral torsional buckling. This failure happens when the beam bends and rotates the entire beam without the deformation of the cross section (Figure 2.4).



a. Sectional view

b. Experimental results (Trahair, 1993)

Figure 2.4 Lateral torsional buckling

Buckle half-wavelength curve and the buckle shape of C section have been shown in Figure 2.5.

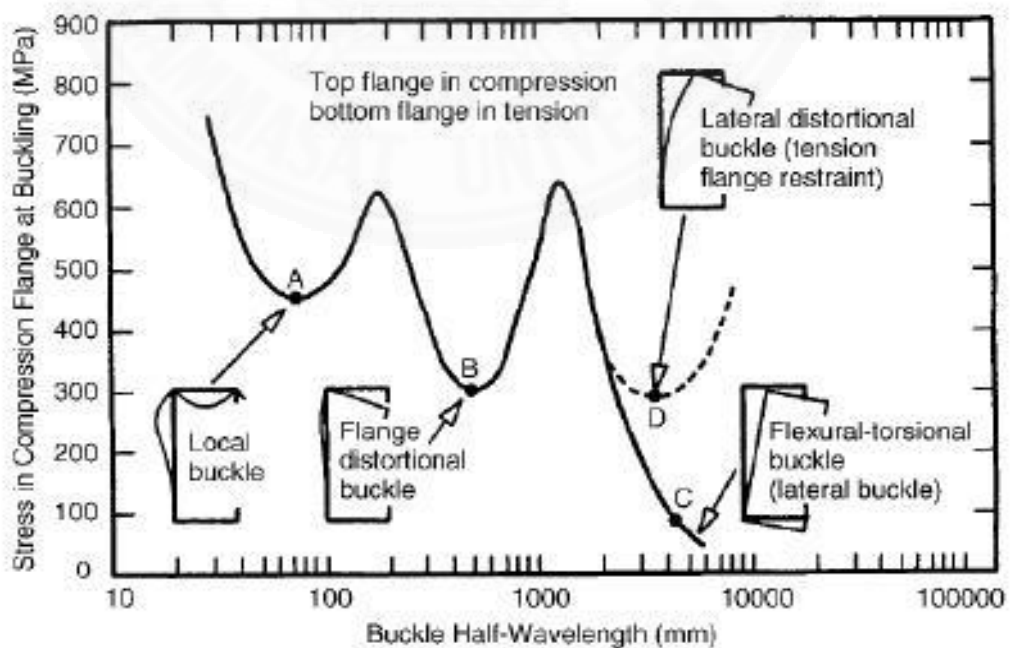


Figure 2.5 Buckling modes of Lipped channel beams in bending (Hancock, 2003)

2.4 Past experimental and numerical investigation on the built-up cold-formed steel beams

- **Experimental study of cold-formed steel built-up C section beam**

Experimental study of cold-formed steel built-up C section beam was studied by H. Thanh Tran, W. Patwichaichote, T. Chaisomphob (2015). Full scale of 4 meter length beam was studied. Influence of connection spacing was the key factor of their study. Two different kinds of section were studied: C15019 and C15024. Moreover, four different kinds of connection spacing were investigated.

Four point bending testing was performed because they wanted to have constant bending moment at the mid-span. The load position approximately equaled to span length over three. Two strain gages at the top flange and two strain gages at the bottom flange were attached at the mid-span. Moreover, one vertical LVDT was placed at the mid-span in order to study vertical deflection at the mid-span. Another LVDT was put laterally at the middle of the span in the aim of studying the lateral movement of the beam, as shown in Figure 2.6 & Figure 2.7. Small and gradual load was applied.

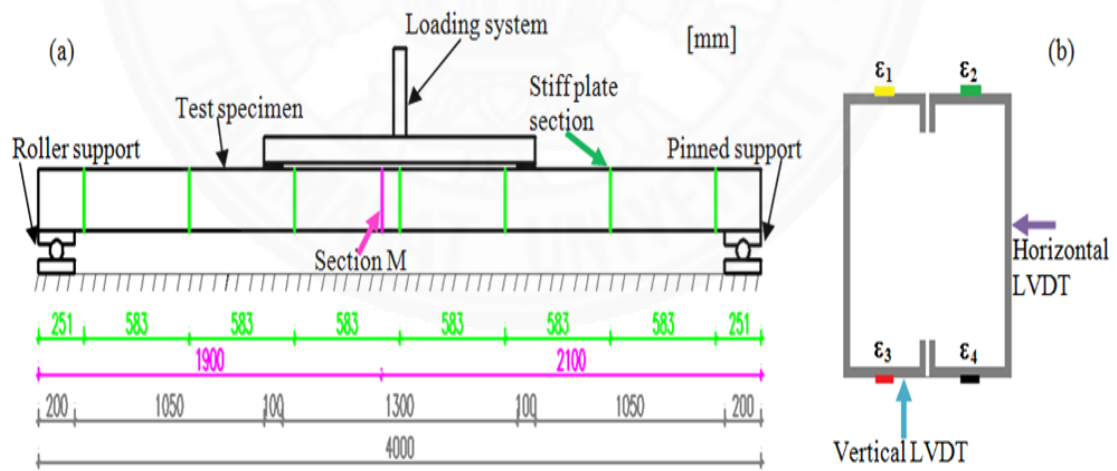


Figure 2.6 (a) Schematic diagram of four-point bending test, (b) Cross section (Tran et al., 2015)

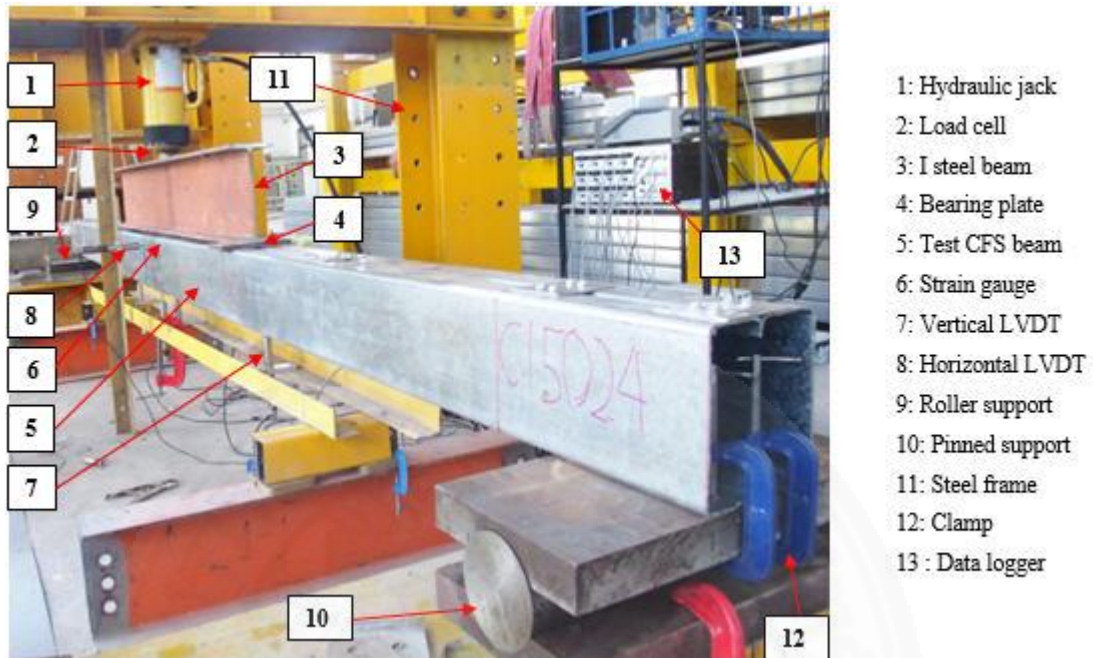


Figure 2.7 Overall view of bending test (Tran et al., 2015)

They found that from specimen with connection spacing $L/2$ to $L/6$, the load capacity of the beam could increase about 10% to 18%. Local buckling was found in specimens having connection spacing $L/6$ and $L/4$. Whereas, $L/3$ and $L/2$ failed in lateral distortional buckling. Numerical study was recommended to verify with the experimental results.

- **Flexural strength of cold-formed steel built-up box sections**

Flexural strength of cold-formed steel built-up box sections was studied by L. Xu, P. Sultana and X. Zhou (2009) and was studied by P. Sultana (2007). Finite element was involved to study flexible strength of their built-up box sections. No guideline or design manual to calculate this kind section (North American Specification). Canadian Standard Association and AISI recommended that moment inertia of built-up equals the sum of two single section based on each deflection compatibility. However, it has not been yet verified by experimental or numerical study. More than 30 specimens were carried out in their study to find the factor affecting the strength. Their test setting up has been shown in Figure 2.8.



Figure 2.8 Built-up box test assembly (Xu et al., 2009)

Concentric and eccentric load can either happen. When one side of the section was loaded and then transferred to another side through the connection or unequal distributed load or torsion, it made eccentric loading. Support floor joist was one of the example.

Beshara and Lawson have performed the experiment to study the influence of position of the screw connection and two types of built-up box sections. The result showed that nominal moment capacity of built-up section is equal 75% of the sum up of the strength of each component.

In their paper, the model was created to verify the experiments conducted by Beshra and Lawson. All beams were made up by C section with either a TD track section or a standard. Half of specimen was considered to grab the benefit of symmetry. The results showed that bracing in lateral could be replaced by lateral displacement $U_x=0$. The shape of local buckling was considered to be symmetrical. Whereas, anti-symmetric buckling response may not be captured in FE analysis.

Their profiles was modeled by the Shell 181 element in ANSYS, while the effect of screws has been dealt by coupling translational and rotational degrees of freedom of the global x, y, and z directions, shown in Figure 2.9.

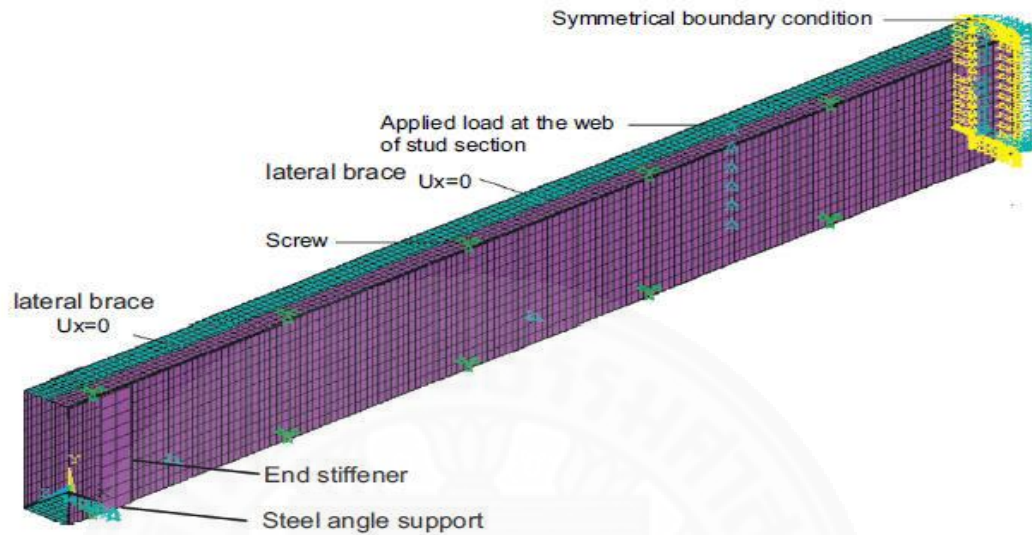


Figure 2.9 Finite element model (Xu et al., 2009)

The effect of residual stress was neglected in their model. Inverted structural steel and roller (no bearing plate) was used to model simple support. Load control and displacement control were used in their study in order to compare between two methods. For load control, 2890N was the apply load that was applied on each node of the screws. The initial load was 347N (max load increment: 867N and min load increment: 2.9N).

Geometry imperfection is very sensitive to the flexural behavior of thin-walled structures. Nonlinear analysis containing imperfection that used scaling first eigenvalue buckling mode shape to represent it was developed in their model in order to get the maximum moment capacity. Changing scaling factor with several of eigenvalue buckling modes was beyond the scope of their study.

Using very small increments have considered for both methods. Their FE analysis result shows that the difference between ultimate load from FE and from the test is 4%. FEA did not have the ability to predict the behavior after reaching maximum load level even using Riks method and refining mesh method. They used 2D surface and 5mm wide bearing plate to replace the inverted angle in practice.

Bonded flexible to flexible contact was used. Local buckling at the flange of the track section and distortional occur both FEA and test, as shown in Figure 2.10.

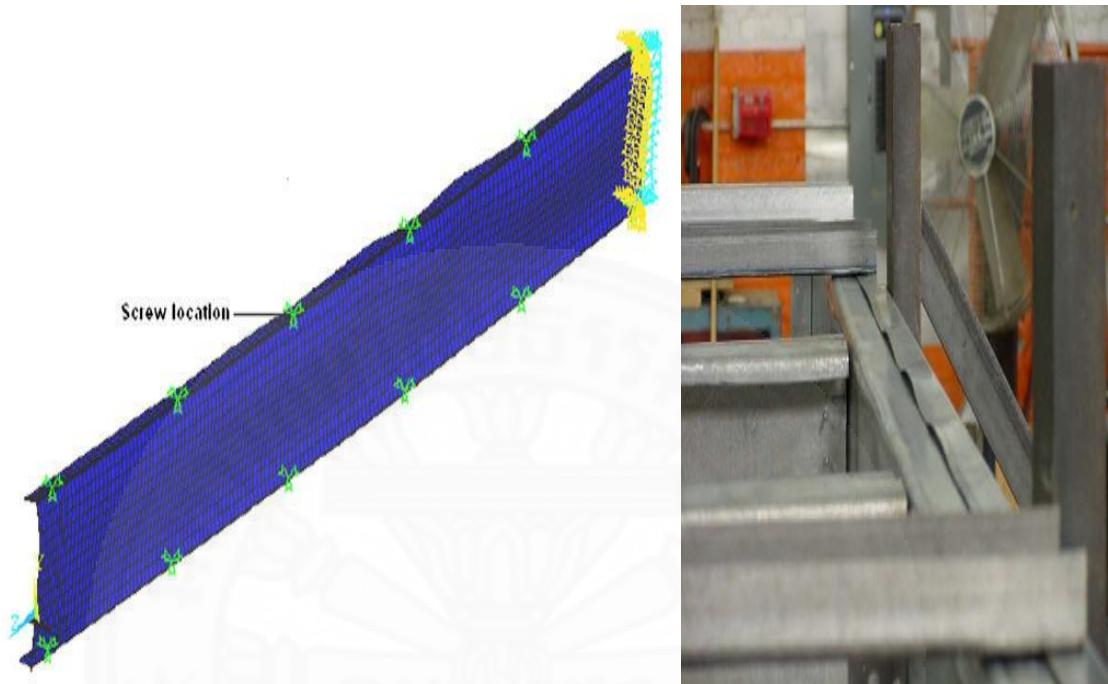


Figure 2.10 Local buckling of compressive flange of track section in FE analysis and the test (Xu et al., 2009)

Their FEA Moment capacity (M_{FEM}) of both procedure is slightly different from the test (M_{test}). It was found that M_{FEM} with support using bearing plate is 21% with TD track sections and 11% with standard track sections greater than inverted angle support. Nominal moment capacities (M_n) are calculated based design manual of North American specification for design of cold-formed steel structural member. Their both test and FEA results show that moment capacities are always lower than the calculation from design manual.

Parametric study

Yield strength and width-to-thickness, effectiveness of the fasteners, and the location of the apply load are really affected to the moment capacities. Parametric in their study are the effects of variation of section depth, steel yield strength, position of applied load, and screw spacing on the moment capacity.

Support condition for their FEA is steel bearing plate and control displacement was applied. Material nonlinearity, initial geometric imperfections, and geometry nonlinearity were considered in their study.

Three different of sections which each of the section has two different yield strengths were conduct to investigate the influence of yield strength on M_{FEM}/M_n ratio in their study. Their result appears to be inconclusive.

$h=203, 254, \text{ and } 305$ mm with $t=1.14, 1.44, \text{ and } 1.81$ mm respectively were used to study about the effect of the depth of section on the M_{FEM}/M_n ratio. Their results illustrate that the current application gives well prediction of the strength for built-up sections with higher h/t ratios for the same section depth.

It does not have the way of calculate of bending strength by the effect of connector spacing in CFS design codes. They used FEA to study the effect of screw spacing with 150mm, 300mm, and 600mm of spacing. Their result shows that the capacity increases when the spacing decreases which might be contribute by the buckling length reduction. Reducing from 300mm to 150mm and from 600mm to 300mm, the flexural strength is increase less than 6%. It shows that the steps recommended by CFS framing design guides offer better approximation of the bending strength for the built-up section of similar spacing of the screw.

Applying loading the concentric loading was studied to find the moment capacities for their FEA. M_n of built-up box section is equal the sum of nominal moment of each section based on the specification. It can see that the current specification is appropriate with the concentric loading.

In their research, numerical analysis was conducted to verify with current practice provided by CFS framing design guides and test result of Beshara and Lawson. Moreover, initial geometry imperfections, material nonlinearity, and geometric nonlinearity were included in their FEA to compared result with the test. It was illustrated that FEA could trustfully predict the flexural capacity as well as the primary and post-maximum load behavior of CFS built-up box sections.

For concentric loading, it is appropriate to assume that the capacity of built up section can assume as the summation of nominal capacity of each individual section. However, for eccentric loading is inappropriate to say that. Factor of 0.9 was their modification that was recommended to be applied to the flexural strength calculated

as the sum of nominal strength of C section and track section. More experiments to verify this study, realistic representation of screws, and consideration of the effect of distortional buckling should be further investigated.

- **Experimental and Numerical analysis on the structural behavior of cold-formed steel beams**

L. Laim et al. (2013) have studied about the structural behavior of cold-formed steel beams which were also one part of L. Laim's work in his PhD thesis (2013). The study of cold-formed steel beam behavior with C, I, box, and double box shaped is presented (Figure 2.11). Four points bending test and FEA were conducted. Their parametric studies were the influence of thickness, height and length of the beam of its structural behavior.

Understanding buckling phenomena of cold-formed steel is the main focus of research field in nowadays. Buckling mode will affect the maximum strength of compressive members as they can happen before parts of cross section yield. Geometric imperfection, high slenderness, and low torsion stiffness are the main factors of the high susceptibility of buckling.

Analytical approximation means and purely numerical analysis were used to study in their field. One example of analytical approximation method is effective width method. In addition, direct strength method and effective section method are examples of combining both analytical approximations and numerical methods. Those two methods are the ways to find flexural capacity and axial compressive of CFS members. EWM reduces plates in local buckling and reduces thickness in distortional buckling.

The aim of their study aim to know the structural behavior of the varying types of beams. With the predictions from available design rules, both results aim to be compared.

For their experiment, 12 specimens with four different kinds of section (C, box, I, and 2box) were carried out and 3 test were conducted for each of the section. Total length of specimen is 3.6 m and its span is 3 m (Figure 2.12). For the connection, connection spacing $L/3$ was used.

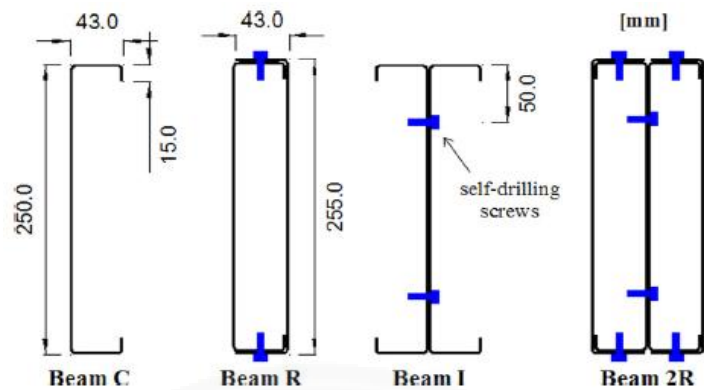


Figure 2.11 The cross-sections of the tested beams (Laim et al., 2013)

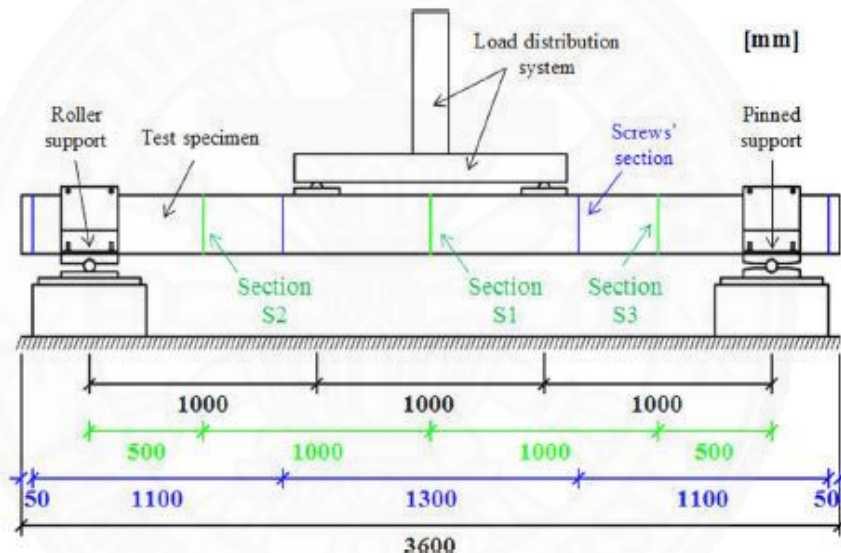


Figure 2.12 Schematic view of the experimental set-up for bending tests (Laim et al., 2013)

In their test, four points bending test at ambient temperature was conducted. Supports prevented vertical displacement, lateral displacement, and lateral rotation of the beam. Moreover, it was free for horizontal displacement for roller support and in contrast for pinned support.

0.01 mm/s rate of displacement control was applied until their specimen buckled and reached its unloading stage. At section S1, S2, and S3, vertical displacement was measured by three LVDTs. Two LVDTs were put to measure the lateral rotation of their specimens at section S1. In order to evaluate the longitudinal strains, a number of strain gages were used around the section S1 and S2. Two LVDTs were placed at the support to determine their rotation.

Beam with double boxes is the highest load capacity in their study. Capacities of I and R are 41.68 and 60.14 kN respectively. The ultimate load of I, box, and double box was over 3.5, 5, and 10 times bigger than the one of C section. Box beam can increase the capacity by 1.45 times of I beam. No plastic plateau was found because of local or distortional buckling may occurred.

In their results, lateral displacement for C is the largest one and the others are small. This is because of the coincidence of the shear center with the centroid, torsional stiffness of compound sections, and increase thickness of the beam cross section.

Their results showed that, for tensile flange, the strains of all beams had the same tendency of each of the section. Whereas, the strain at compressive flange for open section C and I shows a non-uniform increase in the strains.

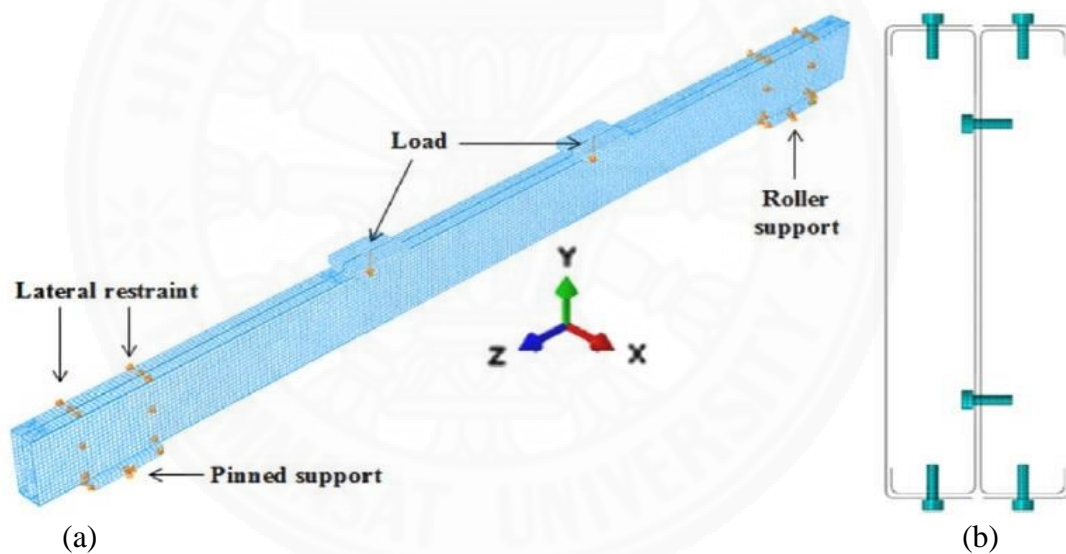


Figure 2.13 Numerical model used in the finite element analysis: (a) perspective and (b) cross-sectional view (Laim et al., 2013)

ABAQUS version 6.10-1 was performed to model their specimens. Shell elements (S4R) were used to simulate the profiles. Moreover, solid elements (C3D8R) were used for the screws (Figure 2.13). Yield strength, tensile strength, and Young's Modulus were equal to 295 MPa, 412 MPa, and 208 GPa respectively. For their finite element mesh, 10x10 mm elements were used for C, lipped I and box beams. For double box, 15x15 mm elements were used. Bearing plate was used to be the support plate. For their contact condition, a tangential friction coefficient of 0.2 was assumed. In addition, between the screws and the profile, a rough and hard contact were another

contact behavior, but between the profiles surface, only hard contact was considered as additional contact behavior.

For their finite element analysis, there were two steps such as linear buckling analysis and nonlinear analysis. Initial geometry imperfection was considered in their model.

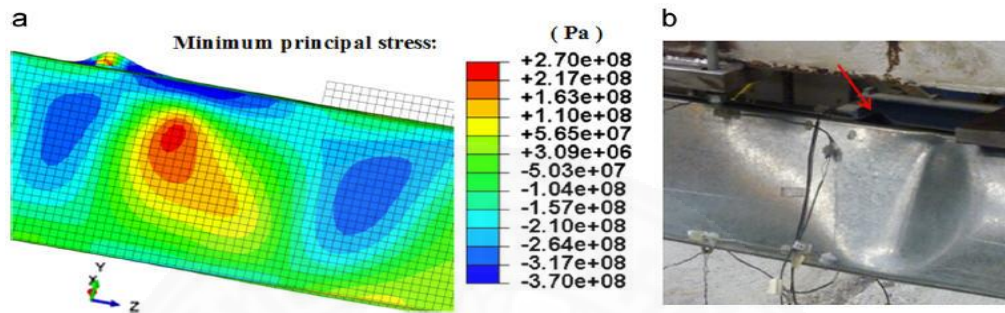


Figure 2.14 FEA (a) and experimental (b) failure modes for the box beam (Laim et al., 2013)

Their result showed that it has a good agreement between the finite element analysis and the test results in term of the flexural strength and failure mode (Figure 2.14).

- **Numerical study on flexural behavior of cold-formed steel built-up C section beam**

Numerical study on flexural behavior of cold-formed steel built-up C section beam was investigated by Tran et al. (2016). Eight specimens was conducted with two different types of section and four different connection spacing. ABAQUS version 6.12 was used to model their specimens, as shown in Figure 2.15.

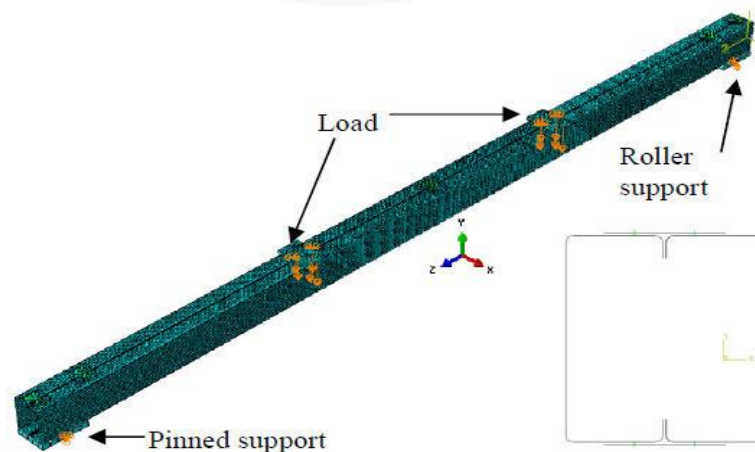


Figure 2.15 FEM model for beam with connection spacing $L/2$ (Tran et al., 2016)

C3D8R and S4R were used to model solid element and shell element in their FEM modeling. Element with 10x10 mm size was applied. In addition, steel material had 485 MPa yield strength and 528 MPa ultimate strength. Young modulus equaled to 200 GPa and Poisson's ratio equaled to 0.3. Two types of contact, surface to surface and tie contact, were used in their interaction modeling. Moreover, there are two procedures in their analysis. First procedure is linear buckling analysis to get the buckle shape. Second is nonlinear analysis with material and geometry non linearity. Their result showed that the FEA results closely matched with the test results for failure mode and also ultimate load capacity of the beam (Figure 2.16). However, it had the different failure mode between numerical and experimental result of the beam with C15024 connection spacing $L/3$.

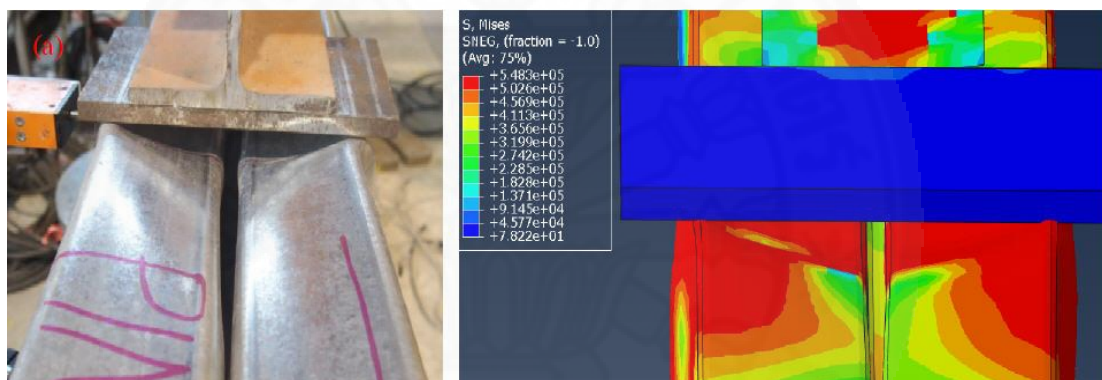


Figure 2.16 Main failure mode comparison between test and FEM test results for C15019 beam with different connection spacing 1750mm (Tran et al., 2016)

- **Behavior of cold-formed steel built-up closed section with intermediate web stiffener under bending**

Manikandan and Sukumar (2016) have studied about behavior of cold-formed steel built-up closed section with intermediate web stiffener under bending. ANSYS program was used to model their model. Nine specimens made-up with two identical C-channel section with intermediate web stiffener were tested and modeled, as shown in Figure 2.17. Those two section connected each other by screws with the 100 mm spacing. Their results showed that flange width and depth of intermediate stiffener were the key affecting the strength and buckling behavior of the member. Their finite element analysis can be used for predicting the load capacity.

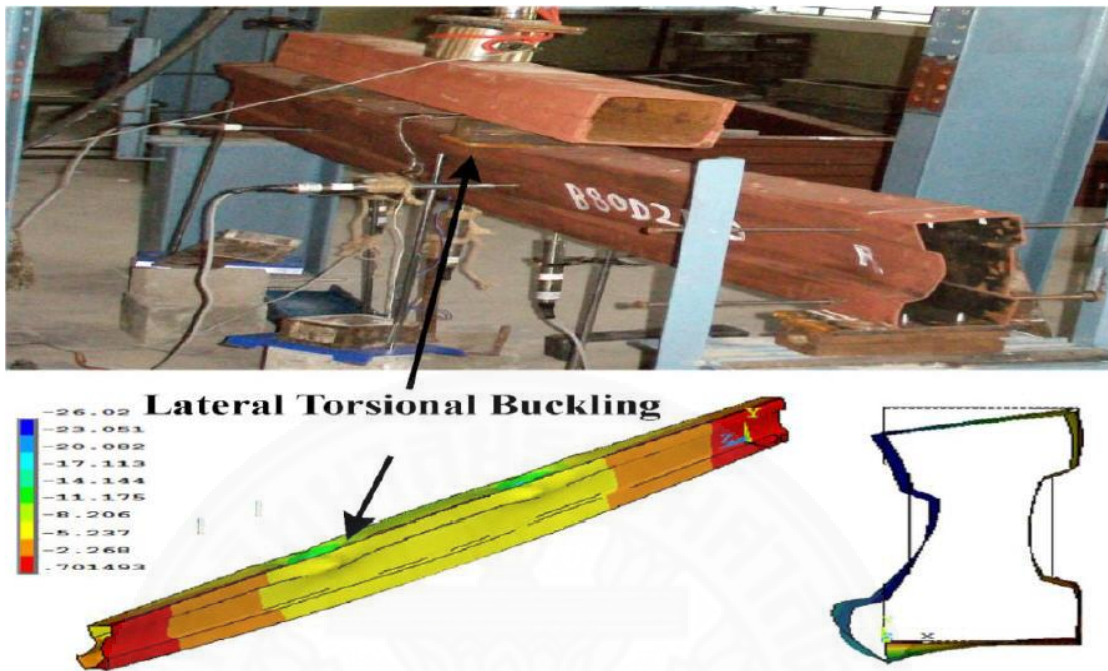
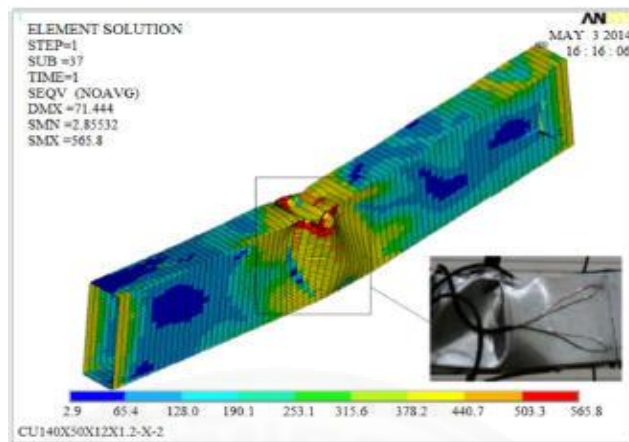


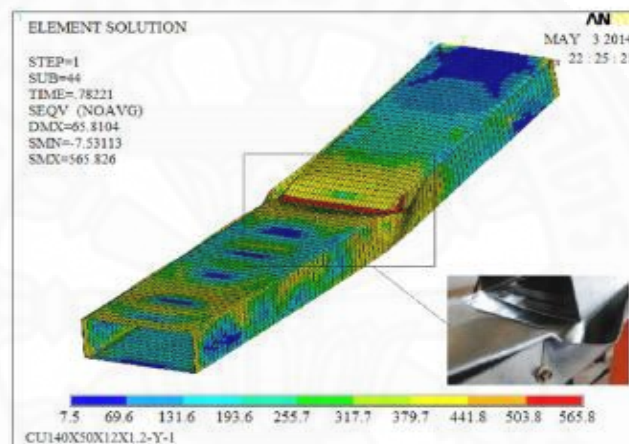
Figure 2.17 Lateral torsional buckling of specimen B4 (Manikandan et al., 2016)

- **Investigation on flexural strength of cold-formed thin-walled steel beams with built-up box section**

Li et al. (2016) have investigated on flexural strength of cold-formed thin-walled steel beams with built-up box section. Seven groups of specimens with three different types of section and 2 bending directions were conducted. ANSYS program was used in their study (Figure 2.18). They have mentioned that sum up method is the accepted method to predict the flexural strength of built-up box beam, but more experiments are important to verify the above method and to fully understand the influence of built-up effect. Their results showed that the moment capacity of the beams bending with the strong axis was suggested equal to 90% of the capacity summation of each component and the equivalent box section can be used for calculation the capacity of the built-up box beam with both strong and weak axis.



(a)



(b)

Figure 2.18 Typical failure modes: (a) CU140x50x12x1.2-X-2, (b) CU140x50x12x1.2-Y-1 (Li et al., 2016)

- **Behavior of cold-formed steel built-up sections with intermediate stiffeners under bending. II: parametric study and design**

Behavior of cold-formed steel built-up sections with intermediate stiffeners under bending. II: parametric study and design was studied by Wang and Young (2016). Finite element model with 113 different built-up section beams was conducted. Numerical results were compared with the experimental results. In addition, direct strength method (DSM) was used in order to compare with those results. Unconservation with current DSM equations for built-up closed section with connectors at flanges was found in their results. The modified DSM equations were recommended.

- **Analytical investigation on cold-formed steel built-up section under flexure**

Raghul and Maheswari (2015) have studied about analytical investigation on cold-formed steel built-up section under flexure. 12 specimens were tested with two different types of section, C and box section. The span length of the beam is one meter long. ABAQUS program was used to model their specimens. Influence of mesh size have beam studied in their research. Finite element mesh with the size of 5x5 mm was applied. They found that the built-up box section beam have failed in distortional buckling.

- **An experimental investigation of stiffened cold-formed C-channels in pure bending and primarily shear conditions**

This study was investigated by Tahir et al. (2015). I section shape that comports from two of C channels with cover plate and without cover plate (Figure 2.19) were studied. Eight specimen have been tested. There were three kind of specimens with different thickness of cover plate (1.6, 2, 2.4 mm) and one kind of specimen without cover plate. Four specimens (3 with cover plate and 1 without cover plate) were subjected to the pure bending test and another four (3 with cover plate and 1 without cover plate) were subjected to shear condition test. Their results showed that the use of cover plate at the top of the section can reduce non dimensional slenderness that improve buckling.

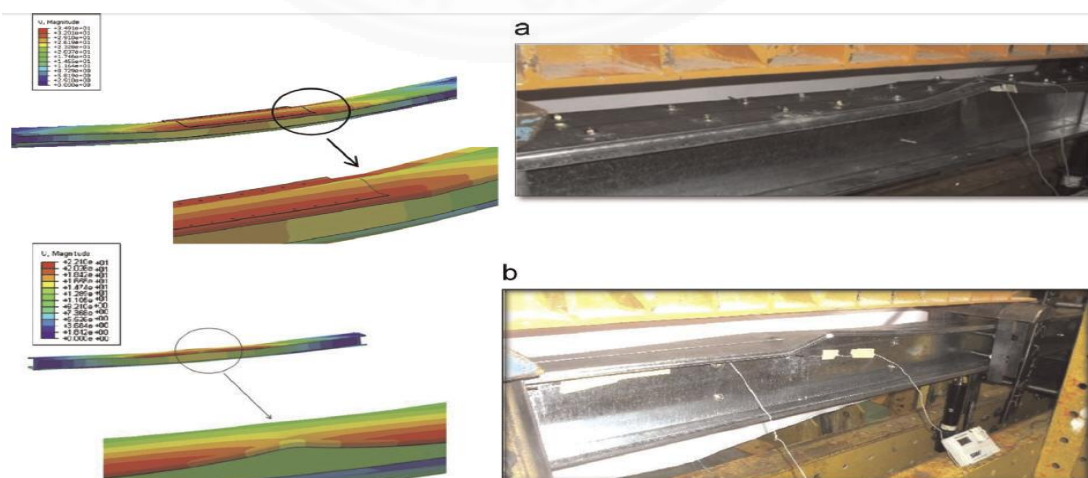


Figure 2.19 A comparison between experimental and numerical (a) local and (b) distortional buckling failure mode subjected to pure bending test (Tahir et al., 2015)

2.5 Computational modeling study

- **Computational modeling of cold-formed steel**

Computational modeling of cold-formed steel was studied by B.W. Schafer, Z. Li, and C. D. Moen (2010). They have studied about the factor sensitivities like element and mesh sensitivity. Cold-formed steel lipped channel column with 1200 mm long were used in their study. The section had the dimensions such as 100 mm web height, 80 mm flange width, 10 mm right angle lip stiffeners, and 2 mm thickness. Young modulus is equal to 210 GPa and yield strength is equal to 345 MPa. In addition, Poisson's ratio was equal to 0.3.

In their study, there were 3 three kinds of element type and density of element mesh, as shown in Figure 2.20. Those element type were S4, S4R, and S9R5. S4 is shell element with 4 nodes and S4R is shell element with 4 nodes and optionally reduced integration. The last element is S9R5 is shell element with 9 nodes which employs quadratic shape functions and reduced integration. On the other hand, three different types of density of element mesh were coarse, medium, and fine mesh. Their result showed that the mesh density had a noticeable effect on the load capacity and failure mode, as shown in Figure 2.21.


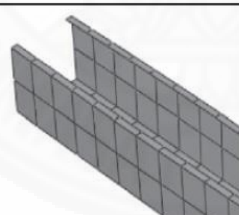
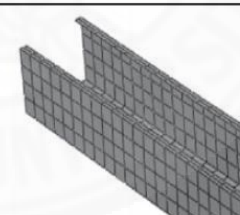
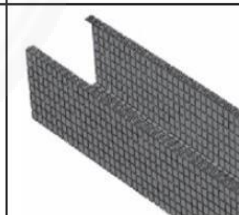
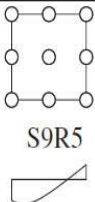
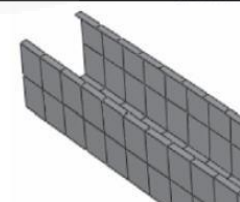
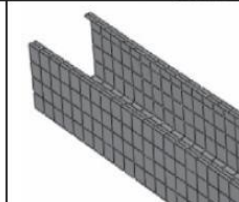
element	coarse mesh	medium mesh	fine mesh
 <p>S4/S4R</p>			
 <p>S9R5</p>	N/A		

Figure 2.20 Element choice (linear and quadratic) and mesh densities for parametric study (Schafer et al., 2010)

Solver sensitivity, plasticity model: sensitivity in ABAQUS, and implementation sensitivity: ABAQUS and ADINA (an alternative to ABAQUS for nonlinear FE collapse analysis) comparison were another factor sensitivities which have discussed in their study. They have found that ABAQUS results are slightly stiffer than the ADINA results.

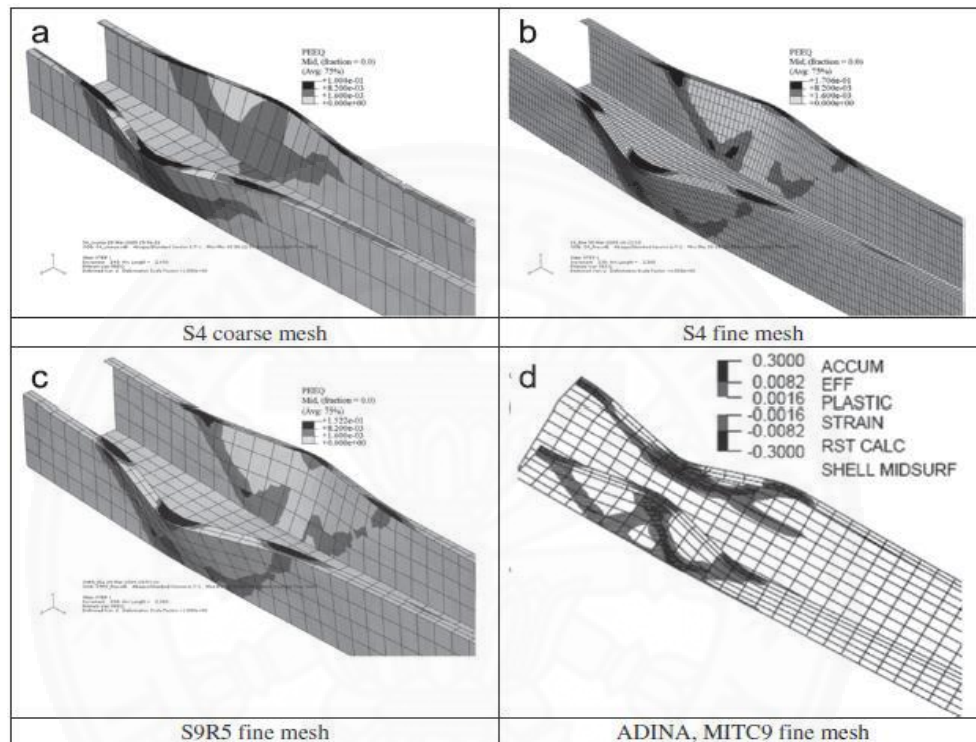


Figure 2.21 Membrane plastic strain, during collapse (at an end shortening 4mm) for different elements and mesh densities (Schafer et al., 2010)

Cold-formed steel computational modeling needs sophisticated mechanics to provide accurate solution. Furthermore, It has an important role to conduct the future research and design of cold-formed steel members.

- **Amplitude of the buckle shape (eigenvectors)**

Linear buckling analysis is very significant for the study on cold-formed steel structure. Linear buckling analysis have performed in order to get the buckle shape. The buckle shape has chosen with the most likely shape that we can recognize in the experiment. After getting the buckle shape, the scale factor was applied in order to scale the buckle shape for getting the initial imperfection shape. The initial

imperfection shape was input in the model in order to analyze the final model with material non linearity and geometry non linearity. The final finite element analysis results have taken to compare with the experimental results. The important parameter in linear buckling analysis is the amplitude of the buckle shape that is either function of the plate thickness or the plate slenderness, as recommended by Schafer (2010).



Chapter 3

Experimental study

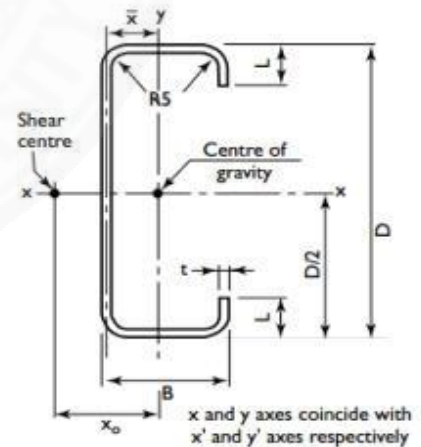
3.1 Experimental method

3.1.1 Material and specimen properties

From the NS Bluescope Lysaght Limited, there are 6 groups of the C section, available as follows: C100, C150, C200, C250, C300, and C350. For each group of section, it has several different thicknesses, from 1 mm to 3 mm. Those sections has the depth from 102 mm to 350 mm with the width from 51 mm to 125 mm. The lengths of CFS products are specified according to customer's need and transportation conditions. Table 3.1 shows the section dimensions.

Table 3.1 Dimension of C section

Catalogue Number	t mm	D mm	B mm	L mm	Mass per unit length(kg/m)
C10010	1.0	102	51	12.5	1.78
C10012	1.2	102	51	12.5	2.10
C10015	1.5	102	51	13.5	2.62
C10019	1.9	102	51	14.5	3.29
C15012	1.2	152	64	14.5	2.89
C15015	1.5	152	64	15.5	3.59
C15019	1.9	152	64	16.5	4.51
C15024	2.4	152	64	18.5	5.70
C20015	1.5	203	76	15.5	4.49
C20019	1.9	203	76	19.0	5.74
C20024	2.4	203	76	21.0	7.24
C25019	1.9	254	76	18.5	6.50
C25024	2.4	254	76	20.5	8.16
C30024	2.4	300	96	27.5	10.09
C30030	3.0	300	96	31.5	12.76
C35030	3.0	350	125	30.0	15.23



The NS BlueScope Lysaght Cee sections are roll-formed from GALVSPAN steel complying with AS1397-1993.

From the results of tensile coupon test, there are three different types of cold-formed steel depending on the thickness of the section:

- 1.2 mm : $F_y = 518.44$ MPa and $F_u = 598.65$ MPa
- 1.5 mm : $F_y = 522.5$ MPa and $F_u = 609.96$ MPa
- 1.9 mm : $F_y = 508.11$ MPa and $F_u = 544.98$ MPa

The stress-strain relationship of CFS with thickness 1.2 mm is shown in Figure 3.1.

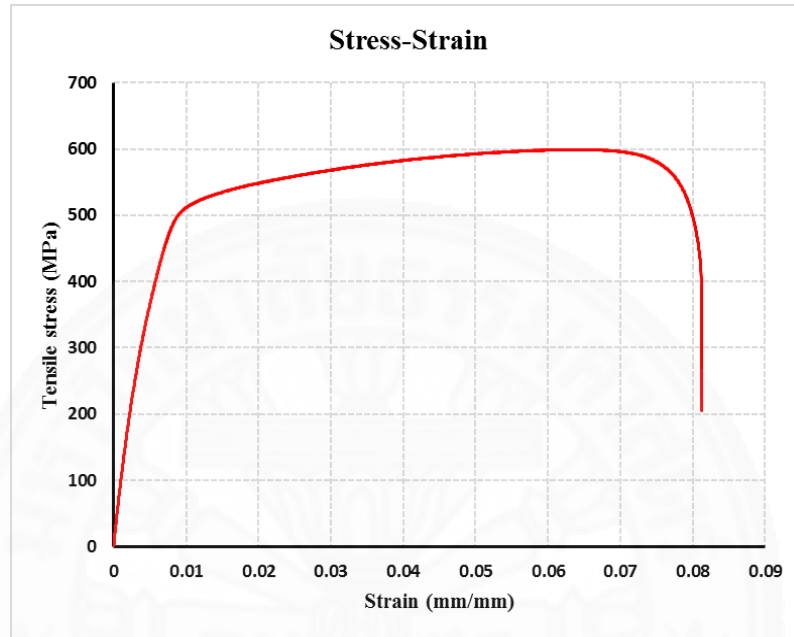


Figure 3.1 Stress-strain relationship of material of thickness 1.2mm

The thickness of cold-formed steel is very thin, and hence screw connection is the most suitable connection. Another reason is that screw connection is easy for installation by the self-drilling process. In this study, the built-up section is connected by using stiffening plate with 4 screws with radius of 1.95 mm.



Figure 3.2 Stiffening plate (80x80x2mm) with 4 screws

In this experiment, there are 20 specimens with 5 different types of section and 4 different connection spacings ($L/2$, $L/3$, $L/4$, and $L/6$). There are five sizes of built-up box with C sections C10012, C10015, C10019, C15012, and C15015 as shown in Table 3.2.

Table 3.2 Details of specimen

Name of Specimen	Name of C section	t (mm)	h (mm)	w (mm)	l (mm)	rs (mm)	Connection spacing(mm)	h/t	w/t
BBC-10012	C10012	1.2	102	51	12.5	5	L/6, L/4, L/3, L/2	85	42.5
BBC-10015	C10015	1.5	102	51	13.5	5	L/6, L/4, L/3, L/2	68	34
BBC-10019	C10019	1.9	102	51	14.5	5	L/6, L/4, L/3, L/2	53.7	26.8
BBC-15012	C15012	1.2	152	64	14.5	5	L/6, L/4, L/3, L/2	126.7	53.3
BBC-15015	C15015	1.5	152	64	15.5	5	L/6, L/4, L/3, L/2	101.3	43.7

*BBC- : Built-up Box C-; t: thickness of C section; h: depth of C section; w: length of flange; l: lip of the C section at the end of the flange; rs: radius of the curve connection between web and flange; L: representative span length (3.5m); $L/6$, $L/4$, $L/3$, $L/2= 583, 875, 1167$, and 1750mm respectively.

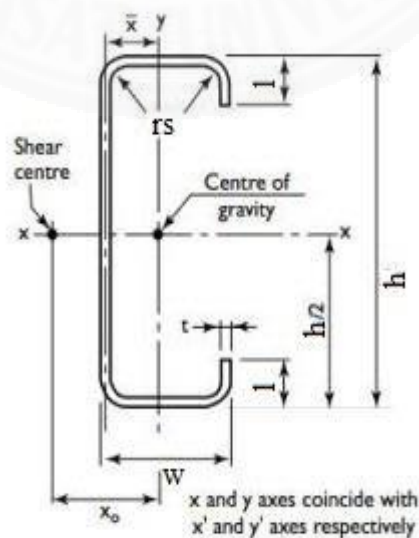


Figure 3.3 Cee cross section

Figure 3.4 and Figure 3.5 are the cross section of the beam specimens.

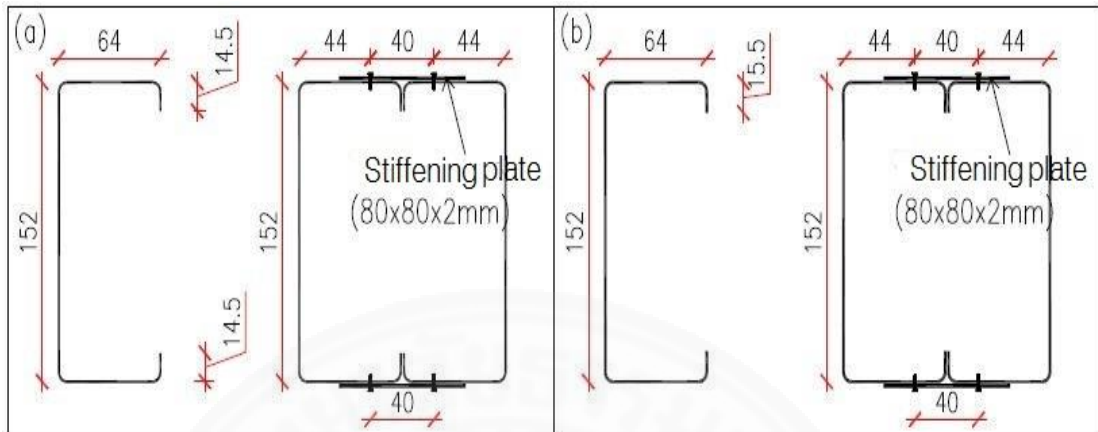


Figure 3.4 Built-up box C section: (a) BBC-15012, (b) BBC-15015

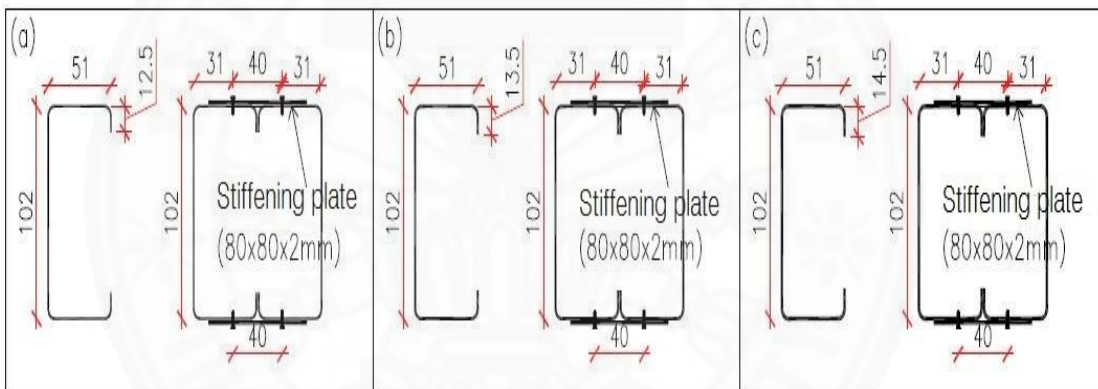


Figure 3.5 Built-up box C section: (a) BBC-10012, (b) BBC-10015, (c) BBC-10019

3.1.2 Test set-up

Figure 3.6 shows the test setting up for the specimen BBC-15012 with the connection spacing equal 1750 mm ($L/2$).

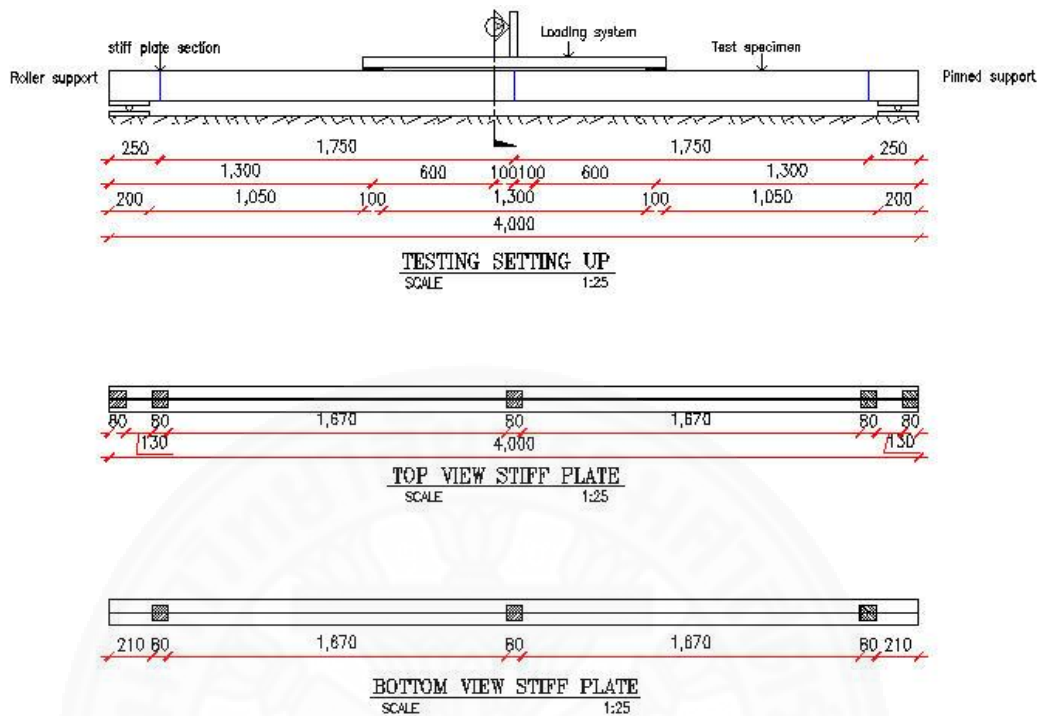


Figure 3.6 Test setting up for BBC-15012 connection spacing 1750mm

At one end of the specimen shown in Figure 3.7(a), a roller support is modeled by a spherical plain bearing to allow only horizontal displacement and the rotation in the plane of bending but to fix the vertical displacement. For another end shown in Figure 3.7(b), it is the pinned support, modeled by a spherical bearing, and by using the clamp to fix the horizontal displacement of the beam.



(a). Roller support



(b). Pinned support

Figure 3.7 Support system

In Figure 3.8, the centerlines of the test specimen are checked in the longitudinal and transverse directions.



Figure 3.8 Checking the centerlines

In Figure 3.9, there are two points of loading that are transferred from I beam, called load-transferring beam. That beam is loaded by hydraulic jack. The position of those two loaded points is 1.2 m from the supports of the beam (nearly one third of the beam span). This system of loading is called four points loading. ENERPAC hydraulic jack, model RR 3014 (see no. 4 in Figure 3.9) is used to apply the load to load-transferring I beam (see no. 6 in Figure 3.9). That hydraulic jack is hung with the steel frame (see no. 8 in Figure 3.9). It is operated by the hydraulic pump. Novatech F204 load cell of 50 kN capacity was put beneath the hydraulic jack and connected directly to the monitor (no. 5 in Figure 3.9). Bearing plate is used to make the point loading distributed along the width of the test beam. Novatech F204 load cell of 50 kN capacity was put beneath the hydraulic jack and connected directly to the monitor (no. 5 in Figure 3.9). Bearing plate is used to make the point loading distributed along the width of the test beam.

1. Roller support
2. Pinned support
3. Beam specimen
4. Hydraulic jack
5. Load cell
6. Load transferring I beam
7. Bearing plate
8. Steel frame
9. Stain gauge
10. LVDT
11. Clamp

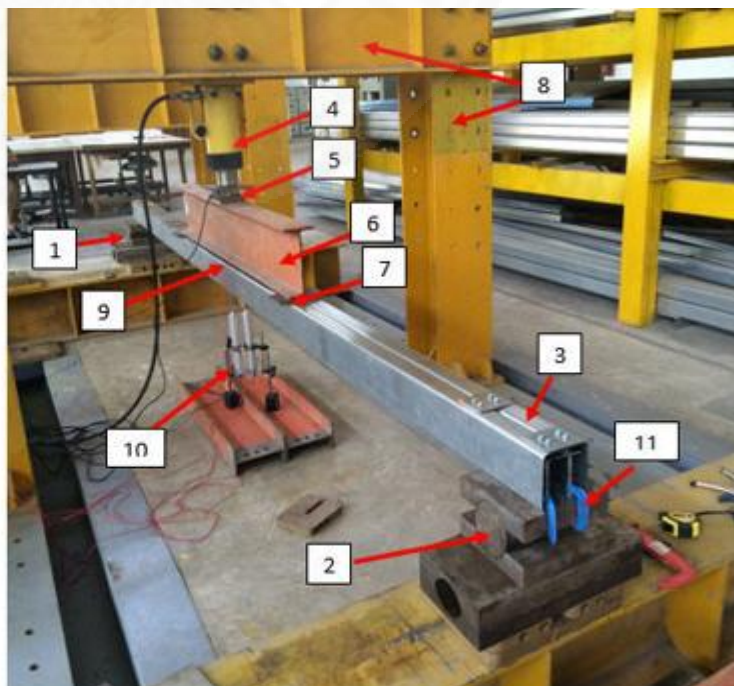


Figure 3.9 Test set-up for four-point bending test

The vertical displacement was measured using linear variable displacement transducer LVDTs of a maximum displacement, 10 cm capacity (no. 10 in Figure 3.9). Figure 3.10 shows strain and vertical displacement measurement at the section A-A 100 mm away from the centerline of the beam specimens (Figure 3.6). Data logger is used to record all the measurement data in Figure 3.11(a), and the load is applied by the controlling with hydraulic pump in Figure 3.11(b).



(a): Strain gage



(b): LVDT

Figure 3.10 Strain and vertical deflection measurement



(a)



(b)

Figure 3.11 (a): Data logger, (b): hydraulic pump

3.1.3 Test procedure

In order to study on the flexural behavior of this cold-formed steel built-up box beam, the experiment is conducted up to the failure of the beam. The test procedure is described by the following steps:

- Prepare machine for testing and check that it works properly or not.
- Prepare beam specimen of the length 4 m
- Set up test by installing the beam specimen, making support conditions, bearing plate, and load-transferring beam.
- Prepare LVDT for measurement vertical deflection and strain gauge at the section A-A 100 mm away from the mid-span. To measure the longitudinal strains, a number of strains gauges were also placed at the section A-A 100 mm away from the mid-span on the top, bottom flange and the web (Figure 3.12).
- Put the load gradually with the time by controlling with the hydraulic pump until the beam fail.
- Use the data logger to record the data for the load, deflections, and stains.

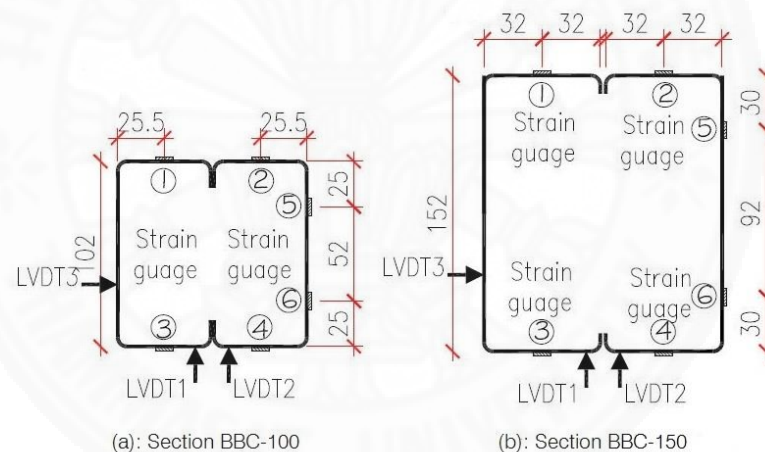


Figure 3.12 Strain gauge and LVDT locations at the section A-A in the tests

3.2 Experimental results and discussion

Table 3.3 illustrates that the flexural load capacity of this built-up box section increases when the thickness increases and connection spacing decreases. For connection spacing $L/6$ and $L/4$, the beam fails in local buckling. For $L/3$, distortional buckling and local buckling was found as the failure mode of the beam. Moreover, the beams that have connection spacing $L/2$ fail in lateral torsional buckling at one side of the C section and distortional and local buckling at another side of the C section.

Table 3.3 Test results

Specimen	Spacing	Failure mode C1	Failure mode C2	Maximum Load(kN)	Δ (mm)
BBC-10012	L/6	LB	LB	9.29	61.38
	L/4	LB	LB	8.32	50.65
	L/3	DB+LB	DB+LB	8.69	54.55
	L/2	LTB	DB+LB	8.25	49.17
BBC-10015	L/6	LB	LB	15.80	72.77
	L/4	LB	LB	15.21	72.52
	L/3	DB+LB	DB+LB	14.53	68.84
	L/2	LTB	DB+LB	11.69	50.86
BBC-10019	L/6	LB	LB	23.00	76.50
	L/4	LB	LB	21.98	84.05
	L/3	DB+LB	DB+LB	20.11	62.62
	L/2	LTB	DB+LB	16.94	54.07
BBC-15012	L/6	LB	LB	17.06	32.23
	L/4	LB	LB	14.3	28.86
	L/3	DB+LB	DB+LB	16.28	33.23
	L/2	LTB	DB+LB	14.21	26.22
BBC-15015	L/6	LB	LB	22.62	38.52
	L/4	LB	LB	22.72	38.19
	L/3	DB+LB	DB+LB	24.98	36.90
	L/2	LTB	DB+LB	23.22	33.94

Δ : Maximum vertical displacement at the section A-A 100 mm from mid-span; L: representative span length (3.5m); C1: one C section side; C2: the other C section side; LB: local buckling; DB: distortional buckle; LTB: lateral torsional buckle; L/6, L/4, L/3, L/2= 583, 875, 1167, and 1750mm respectively.

3.2.1 Influence of web height and flange width to thickness ratio on load capacity

In Figure 3.13, it has two groups of the graphs. The left group is BBC-100 group (BBC-10012, BBC-10015, and BBC-10019) and the right is BBC-150 group (BBC-15012 and BBC-15015). Each group of the graph illustrates that web height to thickness ratio increases, the load capacity of the beam drops dramatically. Height of web is equal to 102 mm and 152 mm for BBC-100 and BBC-150 respectively. Each of the group has the same height, so the thickness is the key factor that influences the ultimate load of the beam. In addition, the load capacity is reduced while connection spacing increases. High web height to thickness ratio of each group of the graph shows the susceptibility to the web buckling of the beam. Figure 3.14 shows the plot of flange width to thickness ratio, and the same tendency is confirmed.

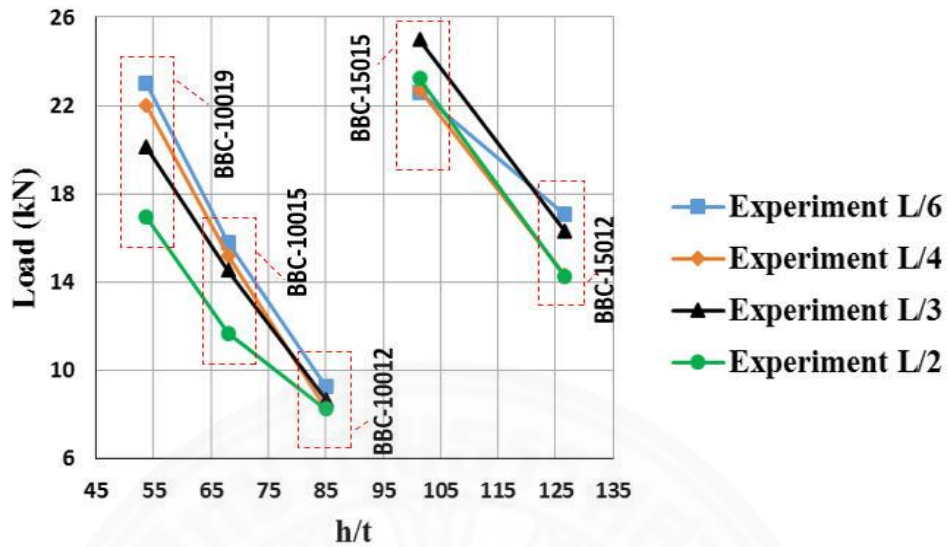


Figure 3.13 Max load-web height to thickness ratio curve for thickness 1.2, 1.5 and 1.9 mm with L/6, L/4, L/3, and L/2

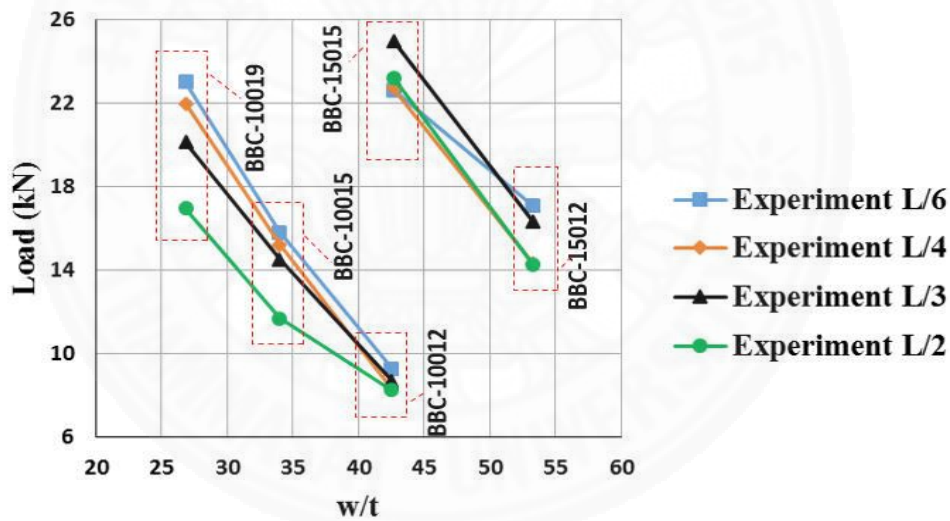


Figure 3.14 Max load-flange width to thickness ratio curve for thickness 1.2, 1.5 and 1.9 mm with L/6, L/4, L/3, and L/2

3.2.2 Influence of the thickness on load capacity

The ultimate load is getting higher when the section have varied from the small thickness to the large thickness (1.2, 1.5, 1.9mm), in case with the same connector spacing. The same tendency was observed in case of connection all spacings (L/6, L/4, L/3, and L/2), shown in Figure 3.15. Changing thickness of the section from 1.2 to 1.5 mm for BBC-100, load capacity of the beam increased in the range of 41.73% to 82.79% and from thickness 1.5 to 1.9 mm for BBC-100, it

increased in the range of 38.35% to 45.55%. Changing thickness of the section from 1.2 to 1.5 mm for BBC-150, load capacity of the beam increased in the range of 32.60% to 63.41%, shown in Figure 3.16. Thickness of the section significantly improved the ultimate load of this built-up box beam.

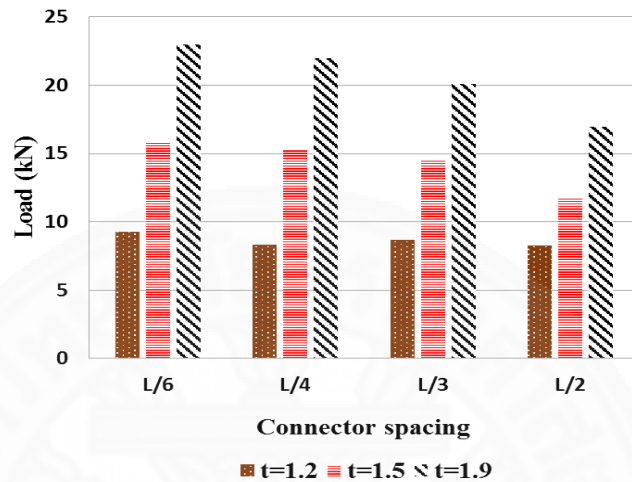


Figure 3.15 Max load associated with variation of thickness 1.2, 1.5 and 1.9 mm for L/6, L/4, L/3, and L/2. (BBC-100)

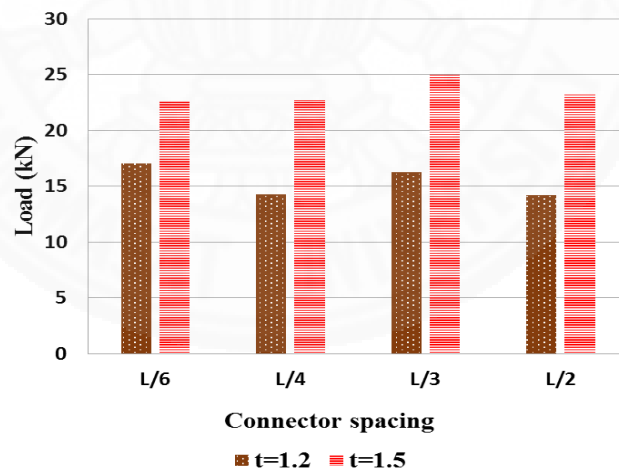


Figure 3.16 Max load associated with variation of thickness 1.2, and 1.5 mm for L/6, L/4, L/3, and L/2. (BBC-150)

3.2.3 Influence of connector spacing on load capacity

Another factor influencing on load capacity is connection spacing. After changing the spacing from the larger to the smaller value (1750, 1167, 875, and 583 mm), the load capacity increases gradually. For instance, BBC-10012 L/2 (1750mm),

the maximum load was 8.25kN. For L/3 (1167mm) with the same section, the maximum load was 8.69 kN. So, from L/2 to L/3, the maximum load increased 5.33% of 8.25kN.

Furthermore, reducing the spacing of the connection from L/2 to L/6 can improve load capacity of up to 35.77% load capacity of L/2 beam. In Figure 3.17 and Figure 3.18, the variation of ultimate load capacity with respect to connection spacings in each group of section is not noticeably different from each other. It can be concluded that the effect of connection spacing on the load capacity is relatively small in comparison with other factors, such as thickness of the section.

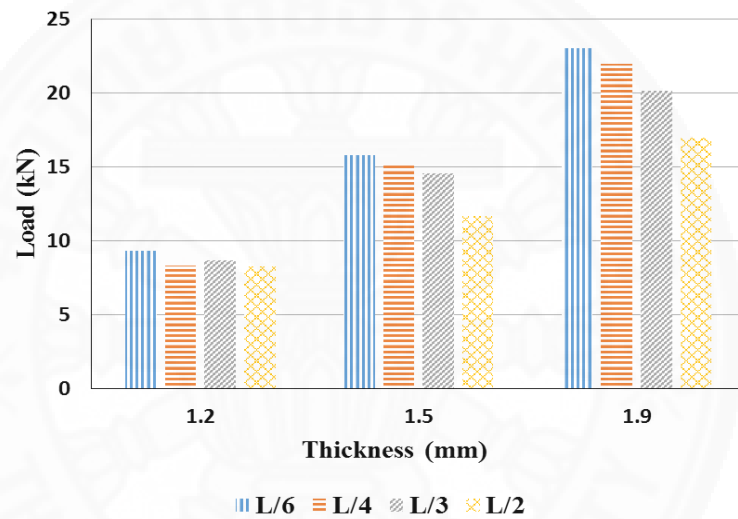


Figure 3.17 Max load associated with variation of connection spacing L/6, L/4, L/3, and L/2 for t=1.2, 1.5, and 1.9mm. (BBC-100)

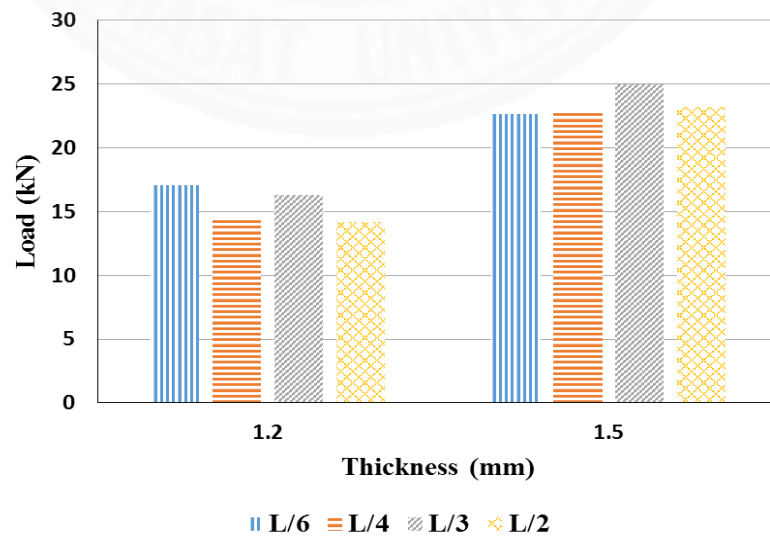


Figure 3.18 Max load associated with variation of connection spacing L/6, L/4, L/3, and L/2 for t=1.2, and 1.5 mm (BBC-150)

3.2.4 Load-deflection curve

Figure 3.19 illustrates the comparison between the load vertical deflection curve of LVDT 1 and LVDT2. The results showed that there are little different between those LVDTs. Thus, the average deflection between LVDT 1 and 2 has been taken as the deflection of the beam as plotted in Figure 3.20.

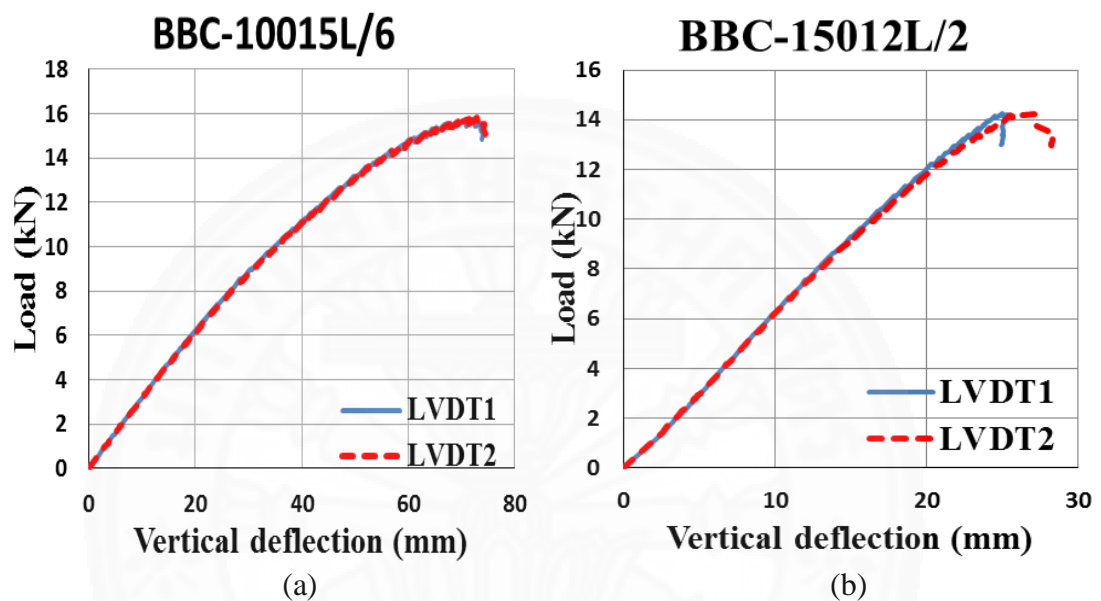


Figure 3.19 Comparison between load-vertical deflection curve of LVDT1 and LVDT2: (a) BBC-10015L/6, and (b) BBC-15012L/2

Figure 3.20 shows that for all five sections, the slopes of load vertical deflection curves in case of different connection spacing are not far different from each other. This confirms that the behavior of the beam is not affected by connection spacing when the load is small or when the beam behavior is in the elastic range. However, the effect of connection spacing is significant at the level of ultimate load, where the behavior becomes nonlinear.

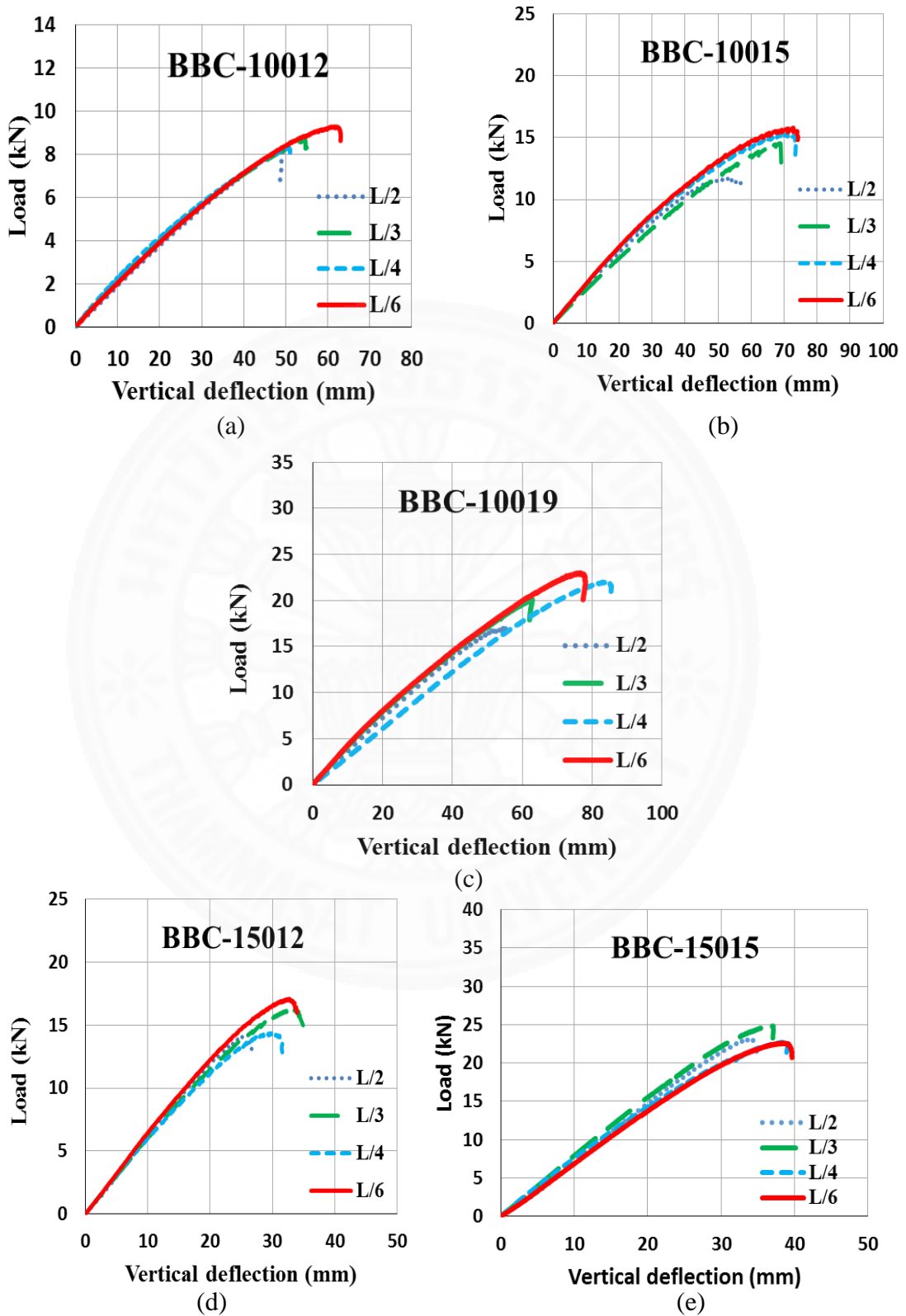


Figure 3.20 Load-vertical deflection curve with connection spacing $L/2$, $L/3$, $L/4$, and $L/6$: (a) BBC-10012, (b) BBC-10015, (c) BBC-10019, (d) BBC-15012, and (e) BBC-15015

Load-lateral deflection curve in case of connection spacing $L/2$, $L/3$, $L/4$, and $L/6$ for built-up box beam with C15015 have been shown in Figure 3.21. For the connection spacing $L/2$ and $L/3$, the lateral deflection increases after reaching the ultimate load. This shows that the beam failed by distortional buckling or lateral-torsional buckling.

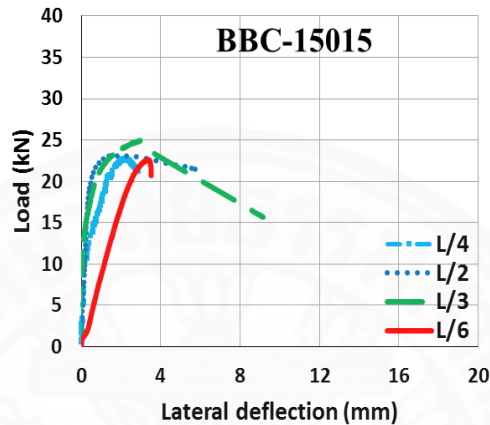


Figure 3.21 Load-lateral deflection curve of BBC-15015 with connection spacing $L/2$, $L/3$, $L/4$, and $L/6$

3.2.5 Load-strain curve

Strain 5 and 6 are on the web the C section, and strain 1 and 2 are on the top flange and strain 3 is on the bottom flange (Figure 3.12). Load-strain curves of the web 5 and 6 fall in between the load-strain curves of the top and the bottom 1, 2, and 3 flange (Figure 3.22).

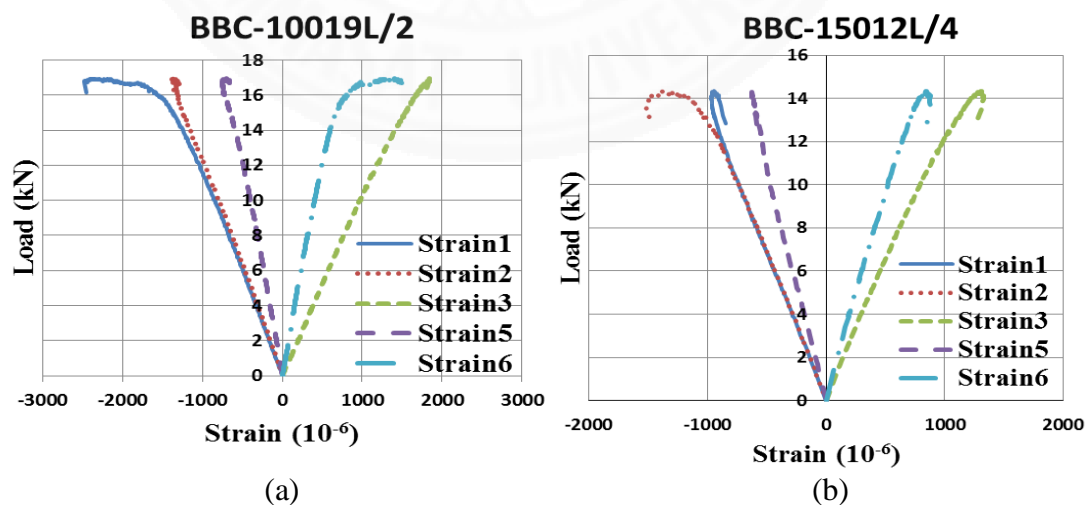
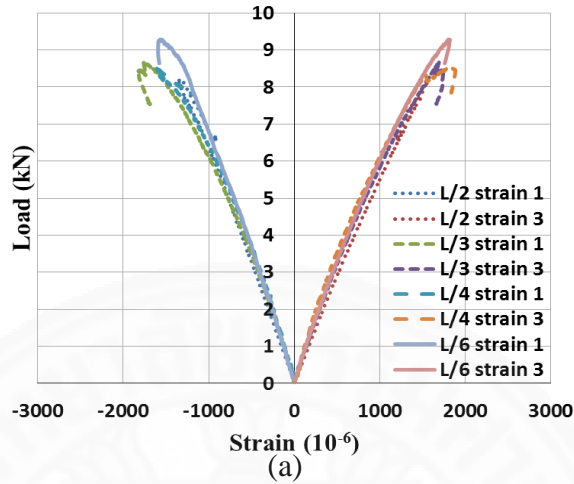


Figure 3.22 Load-strain curve of section A-A 100 mm away from mid-span: (a) BBC-10019L/2, and (b) BBC-15012L/4

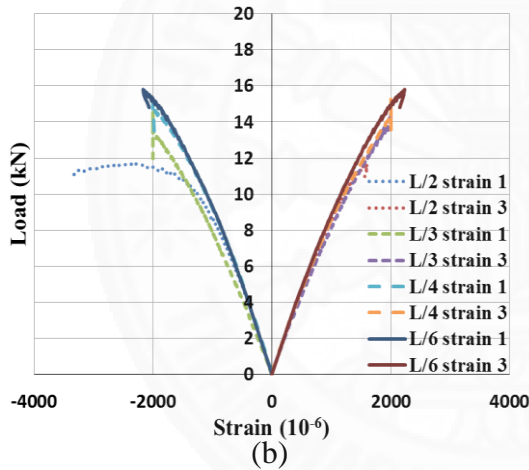
For all 20 specimens, the curves of strain versus load were illustrated in Figure 3.23. For the same section with different connection spacings, the curves of the load-

strain have almost the same slope, and the compressive strain occurs on the top flange, while the tensile strain occurs on the bottom flange. This confirms that the elastic behavior occurs at the measured section closed to the mid-span of the beam.

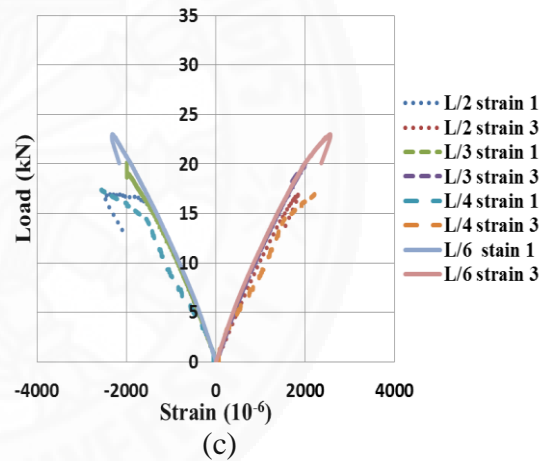
BBC-10012



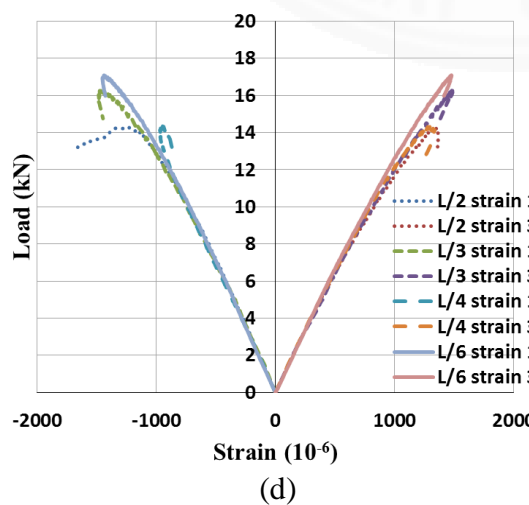
BBC-10015



BBC-10019



BBC-15012



BBC-15015

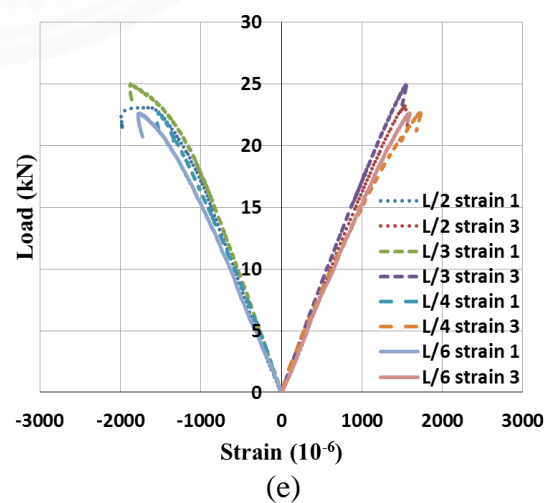


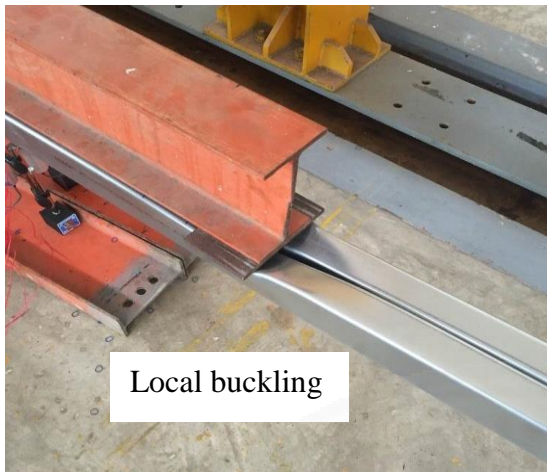
Figure 3.23 Load–strain curve with connection spacing L/2, L/3, L/4, and L/6: (a) BBC-10012, (b) BBC-10015, (c) BBC-10019, (d) BBC-15012, (e) BBC-15015

3.2.6 Failure mode

Figure 3.24 to Figure 3.28 show the failure modes of the beam BBC-10012, BBC-10015, BBC-10019, BBC-15012, and BBC-15015. Each of the figure contains the photos of the different modes according to four connection spacings. It is observed that the beams with the same connection spacing failed in the same failure mode, but the position of the failure could be slightly different. All details are shown in Table 3.3.



Figure 3.24 Failure mode of BBC-10012



(a) Connection spacing $L/6$



(b) Connection spacing $L/4$



(c) Connection spacing $L/3$



(d) Connection spacing $L/2$

Figure 3.25 Failure mode of BBC-10015



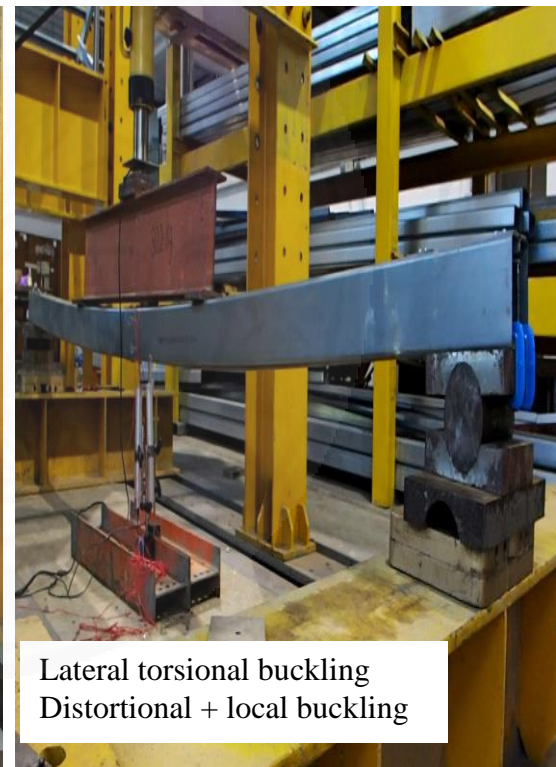
(a) Connection spacing $L/6$



(b) Connection Spacing $L/4$

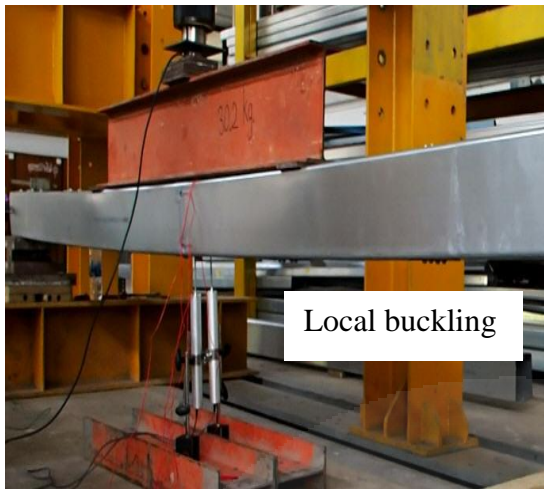


(c) Connection spacing $L/3$



(d) Connection spacing $L/2$

Figure 3.26 Failure mode of BBC-10019



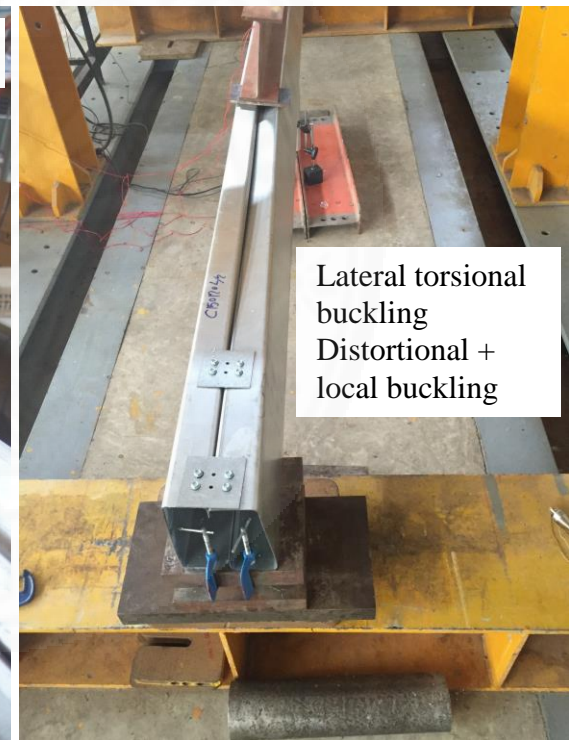
(a) Connection spacing $L/6$



(b) Connector spacing $L/4$



(c) Connection spacing $L/3$



(d) Connection spacing $L/2$

Figure 3.27 Failure mode of BBC-15012



Figure 3.28 Failure mode of BBC-15015

In summary, total of 20 specimens of built-up box beam that contains five different types of section and four different connection spacing. The sections were BBC-10012, BBC-10015, BBC-10019, BBC-15012, and BBC-15015. The connection spacing was set as L/2, L/3, L/4, and L/6. Comparing load capacity of the L/2 beam

and L/6 beam, maximum load can increase in range up to 35.77% of L/2 beam. In addition, increasing thickness from 1.2 to 1.5 mm for BBC-100, maximum load of the beam increases 41.73% to 82.79%. For 1.5 to 1.9 mm for BBC-100, it increases from 38.35% to 45.55%. Moreover, changing thickness from 1.2 to 1.5 for BBC-150, ultimate load get higher in the range of 32.60% to 63.41%. The beams with connection spacing L/6 & L/4 failed with local buckling, whereas the beam with connection spacing L/3 & L/2 are failed with distortional buckling, lateral torsional buckling, and some local buckling.



Chapter 4

Numerical study

4.1 Numerical method

In chapter 3, experimental study is accomplished to obtain the failure mode of the beam and its load capacity. In this chapter, finite element analysis by using ABAQUS program was carried out in order to compare the numerical results with the experimental results. Moreover, influence of thickness, connection spacing, and web height and flange width to thickness ratio on the ultimate load and failure mode of the beam will be discussed.

4.1.1 Element type

The thickness of C section, 1.2, 1.5, and 1.9 mm, are quite small compared to the dimension of the section. Another component is stiffening plate with 2 mm thickness. When one dimension is very small compared with other two dimensions, shell element based on Kirchoff theory is recommended. Shell element was used to model C section and stiffening plate because their thickness is very small. The conventional stress/displacement shell with 4 nodes and optionally reduced integration (S4R) was used (Figure 4.1). Load and support bearing plate have quite large thickness in comparison with other two dimensions, and were modeled by using solid elements (C3D8R), shown in Figure 4.1. In this study, screws are not modeled by 3D elements, for the sake of simplicity.

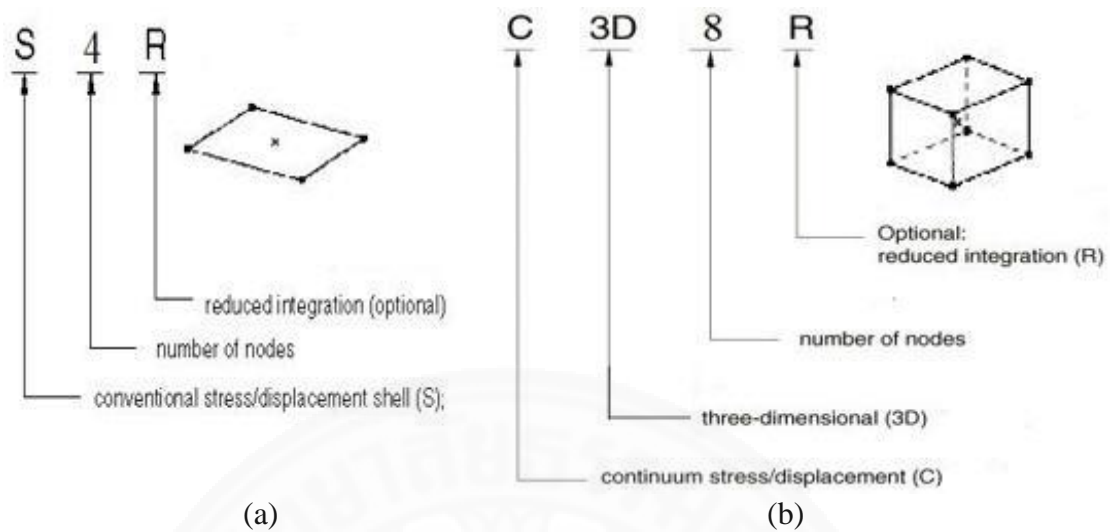


Figure 4.1 The meaning of index representation: (a): Shell element, (b): Solid element

4.1.2 Material properties

Plastic stress-strain relation or material nonlinearity was considered for the C sections. Failure at the stiffening plate was not found in the test of all 20 specimens. Therefore, elastic behavior was assumed for the stiffening plate. Moreover, rigid material with value of thousand time greater than that of normal steel was considered for load and support bearing plate. From results of tensile coupon tests in Chapter 3, There are three different types of yield strength and ultimate strength of the cold-formed steel beam specimens depending on the thickness of the section: 1.2 mm: $F_y = 518.44$ MPa and $F_u = 598.65$ MPa, 1.5 mm: $F_y = 522.5$ MPa and $F_u = 609.96$ MPa, and 1.9 mm: $F_y = 508.11$ MPa and $F_u = 544.98$ MPa. The other properties are young modulus of steel = 208 GPa, and Poisson's ratio = 0.3.

4.1.3 Fastener and contact condition

From the test results, the failure of the screws does not occur. Thus, the simple model called as "fastener" in ABAQUS program was used to model the connections. At the location of the screws, nodes were constrained all translational and rotational degrees of freedom. The radius of screw was equal to 1.95 mm and used as the radius dimension in ABAQUS program (Figure 4.2).

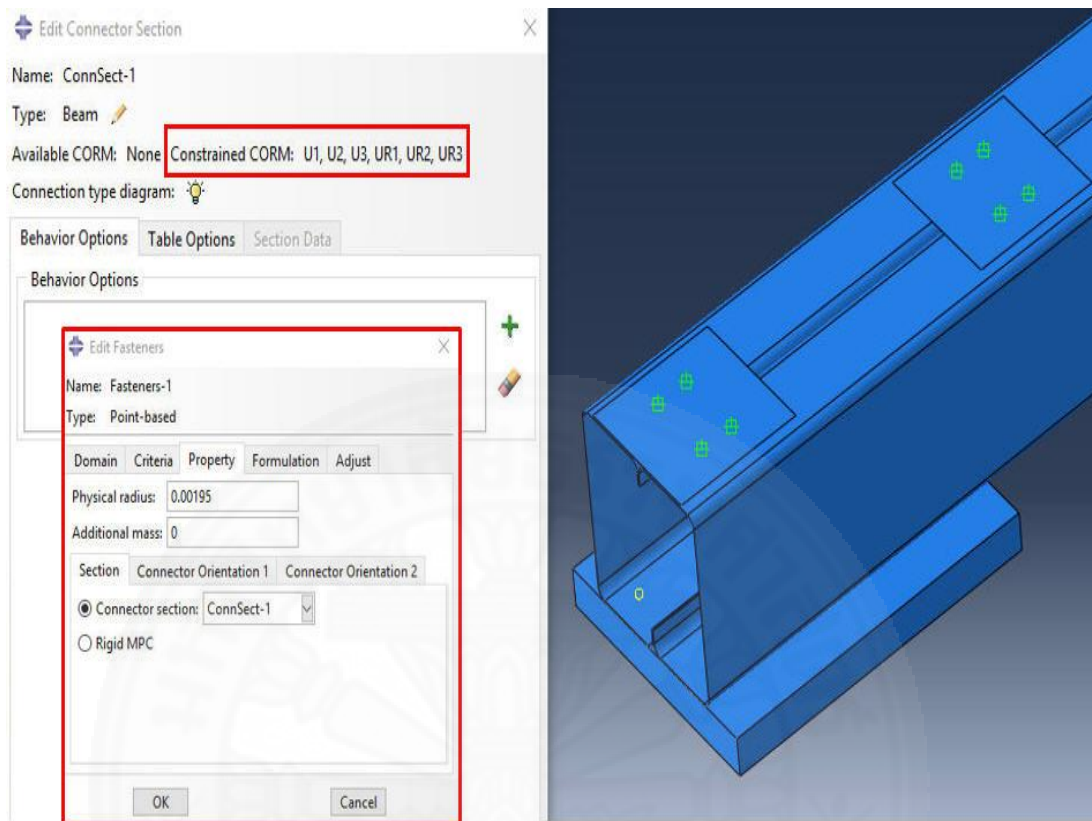


Figure 4.2 Screw connection modeling

At the location of lips of both C sections, one C section side of the built-up box section touched another C section side during the test. Hence, the contact between lips of both C sections was considered in the finite element model. Load was transferred from the hydraulic jack through the load cell and load-transferring I beam. Then, load-transferring I beam distributes the load through the load bearing plates that were beneath its both end. After that, load bearing plate transferred the load to the beam specimen. Contact behavior between the load bearing plate and the beam have to be considered carefully. Contact between lips of both C sections and contact of load bearing plate with the beam were modeled by using surface to surface contact. In order to create the contact, first, the interaction properties have to be created. The property with finite sliding, frictionless, “hard” contact pressure over closure properties was used. Second, master surface and slave surface need to be defined. For contact lip and lip, either one side of the lip can be chosen as master surface and another side as slave surface, shown in Figure 4.3. For contact between load bearing plate and the beam in Figure 4.4, the master surface was the bottom surface of the

load bearing plate and the slave surface was the flange surfaces that touched with the bottom surface of the load bearing plate. However, the slave surface of the contact between the load bearing plate and the beam was extended 2 cm each side of the load plate (Figure 4.4). This extension of contact was observed in the test.

Moreover, tie contact was used to account for the interaction between the support bearing plates and C sections in Figure 4.5. For tie contact, interaction properties does not need to be created. Surface on the top of support bearing plate was the master surface and the flange surfaces that touched with support bearing plate were the slave surface in ABAQUS model.

One important thing when choosing the slave surface of the shell element is that the right side of the surface has to be chosen.

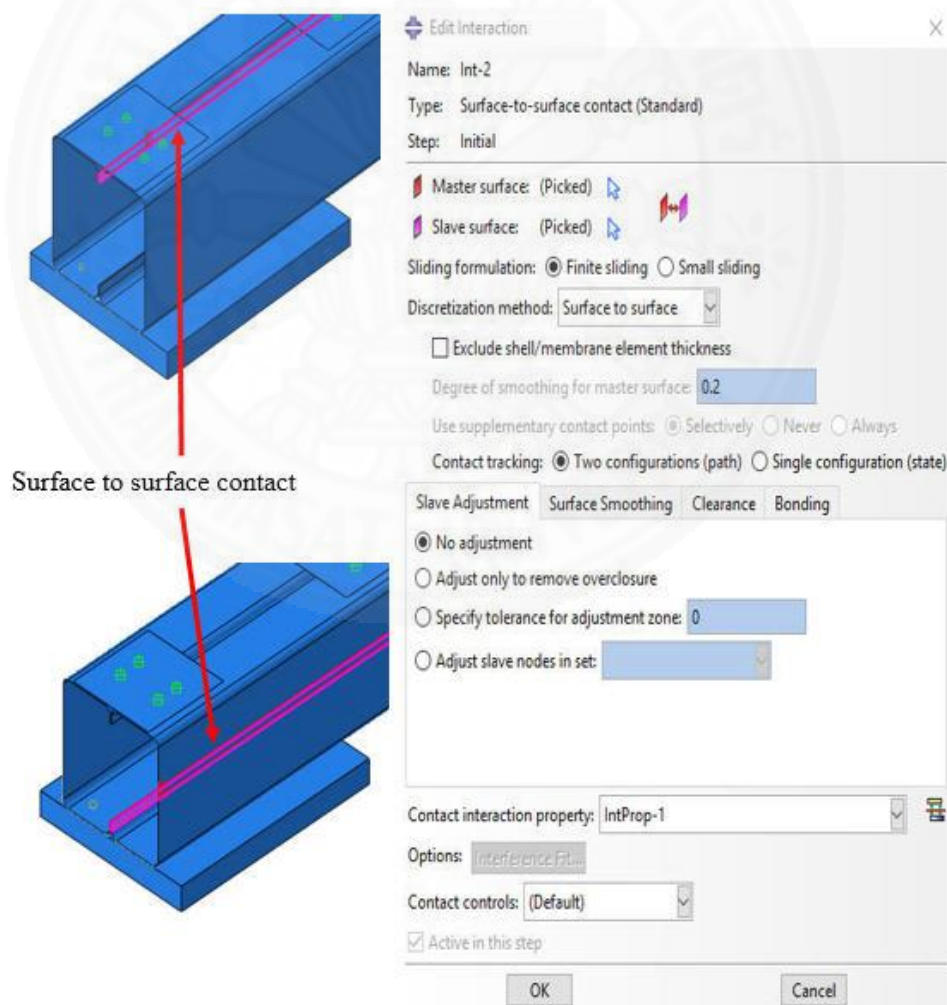


Figure 4.3 Surface to surface contact of lip with lip

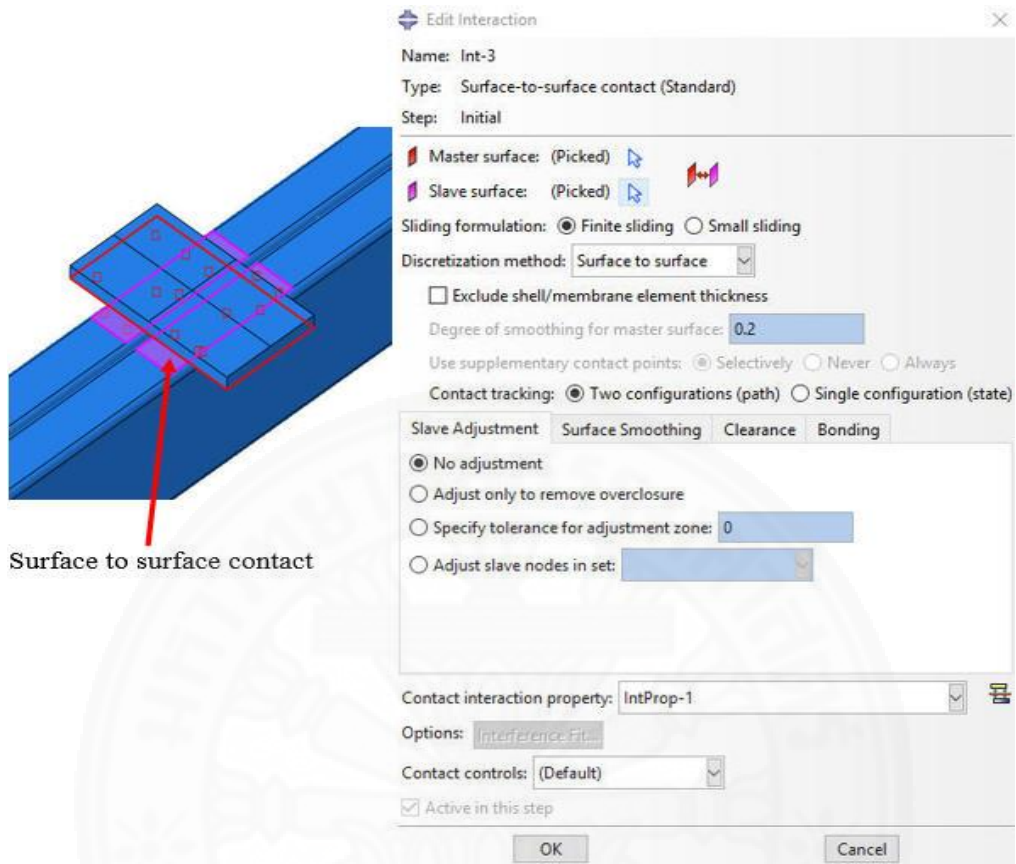


Figure 4.4 Surface to surface of load bearing plate with C sections

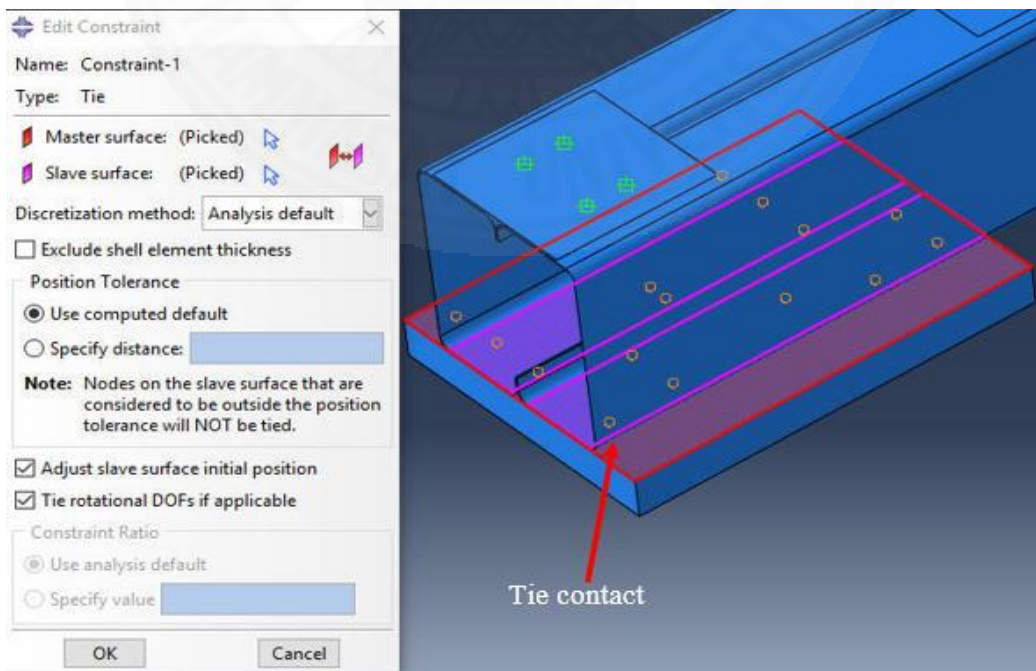


Figure 4.5 Tie contact between C sections and the support bearing plate

4.1.4 Boundary and loading

For the test set-up, at both end of the beam specimen, the steel supports were installed. The box beam section was above the steel plate of the support, as shown in Figure 3.9. In addition, in order to distribute the load from load-transferring I beam to the beam section at two points, load bearing plates were used (Figure 3.9).

On the bottom surface of the support bearing plate, a middle line was drawn in order to specify the conditions of roller and pinned support. For pinned support, all translations of the nodes were constrained (X, Y, and Z axis). Whereas, the translations in the directions X and Y were constrained to model roller support. In the real test, vertical load was applied on the beam. However, controlled displacement was used in finite element analysis in order to trace the softening part of the load-deflection curve. Top surface of the load bearing plates was divided into 4 equal areas by drawing the two middle lines of the plate in the direction of the X and Z axis (Figure 4.6). Vertical Y displacement was applied along those lines. There were additional restraints in X and Z direction located at both ends of the line parallel to Z axis, shown in Figure 4.6.

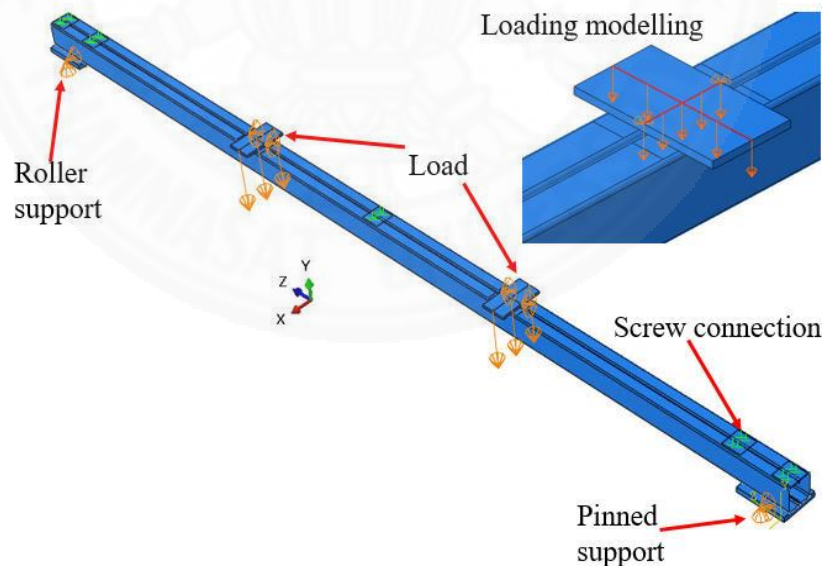


Figure 4.6 Support conditions and loading modeling

4.1.5 Finite element mesh

To accurately study the behavior of the beam up to failure requires a good selection of finite element mesh in modeling. The fine mesh and square shape to

avoid the distortion of the element shape were recommended. The shell element mesh with size of 7.5 x 7.5 mm were used to model the box sections and stiffening plates. The size of solid element for load bearing plate is 7.5 x 7.5 x 10 mm. The cubic element of 20 x 20 x 20 mm size was used to model the support bearing plates. Three divisions were applied in order to get more accurate results for the curve at corner of the C section and the lip. Figure 4.7 shows the mesh of the corner curves and the lips of the C sections.

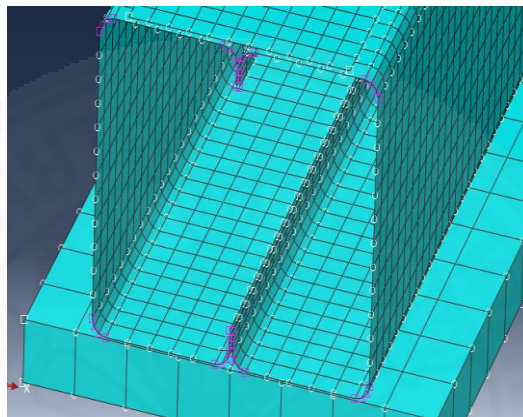
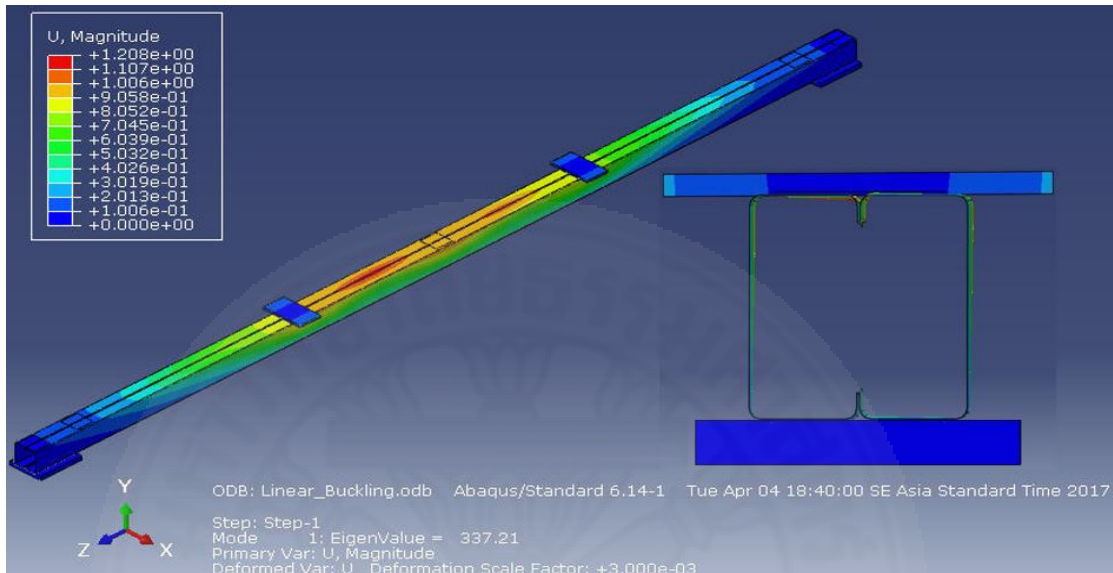


Figure 4.7 Mesh of corner curves and lips of C sections

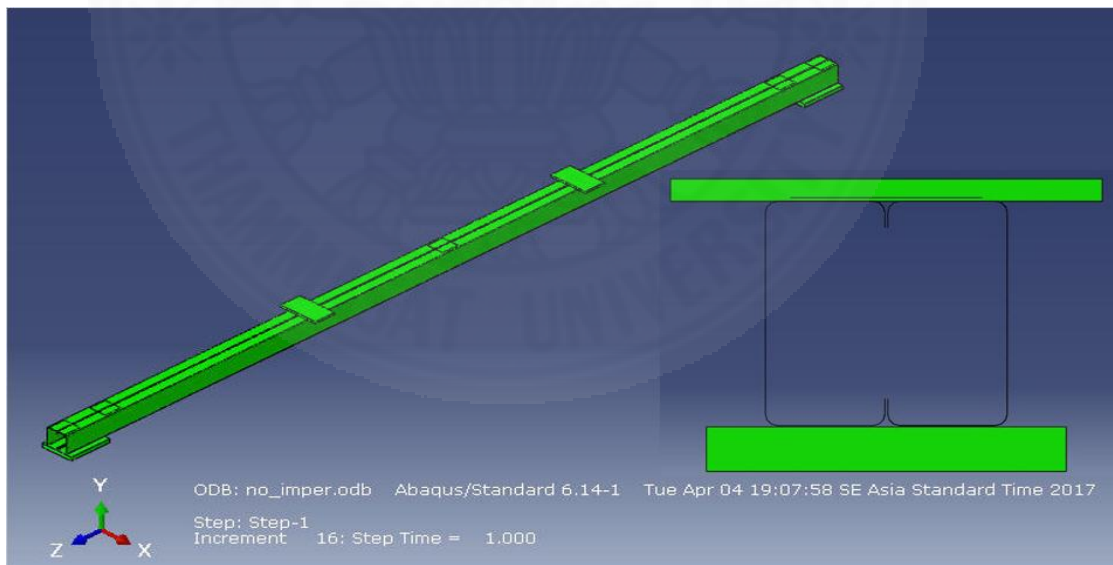
4.1.6 Analytic procedure

In the present numerical analysis, the geometric imperfections were considered. Eigen value buckling analysis or linear buckling analysis was used to obtain the buckling mode shape (eigenvectors). The buckling shape has been used to represent initial imperfection shape with scale factors. The first mode from linear buckling analysis was selected as the mode shape. Figure 4.8 shows about the comparison of the shape between section with imperfection and no imperfection from the section view and whole shape of the beam view of BBC-10012L/2. Deformation scale factor equal to 0.003 was applied shown in this figure in order to see more clearly about the buckle shape. The real scale factor applying on the buckling shape was equal to the shell thickness. Figure 4.8 shows that the section rotates and it has some buckles at the top flange with section imperfection and the beam fails in distortional buckling and lateral torsional buckling for this connection spacing L/2. For the other connection spacing of BBC-10012, the beams fail in distortional buckling. The same tendency was confirmed with other sections. After modeling the beam specimen with

initial imperfection, a general static analysis including geometric and material nonlinearity was performed to obtain the load-deflection relation of the beam. Function of nonlinear geometry (NLgeom: On) was set to deal with nonlinear effects of large displacements.



(a) Section with imperfection (Deformation scale factor 0.003)



(b) Section no imperfection

Figure 4.8 The comparison of the shape between section imperfection and no imperfection for BBC-10012L/2

4.2 Numerical results and discussion

Table 4.1 illustrated the results of finite element analysis in comparison with experimental results. The ultimate load, vertical displacement at failure, and failure

mode are shown in this Table. It can be seen that the difference between ultimate load from FEA and the experiment was between -15% and +12% and the difference between vertical displacement at failure from FEA and the experiment was between -19% and +20%. For larger section like BBC-15012 and BBC-15015, the failure modes from numerical analysis and the test have found to be the same with all kinds of connection spacing. However, failure modes between FEA and the test of smaller sections BBC-10012, BBC-10015, and BBC-10019 in case of connection spacing L/6, L/4, and L/2 were similar. On the other hand, for these smaller sections in case of connection spacing L/3, FEA results showed that the beams failed in local buckling. In contrast, from the test results, the failure mode was distortional and local buckling. It is noted that from the FEA results, ultimate load capacity mostly increased when connection spacing decreased, and the increase of thickness considerably affected the ultimate load capacity.

Table 4.1 FEA results and test results

Specimen	Connection spacing (mm)	FEA results				Experimental results				$\frac{P_{FEA}}{P_{max}}$	$\frac{\Delta_{FEA}}{\Delta_{max}}$
		P_{FEA} (KN)	Δ_{FEA} mm	Failure mode		P_{max} (KN)	Δ_{max} mm	Failure mode			
				C ₁	C ₂			C ₁	C ₂		
BBC-10012	L/6	9.73	57.78	LB	LB	9.29	61.38	LB	LB	1.05	0.94
	L/4	9.34	53.10	LB	LB	8.32	50.65	LB	LB	1.12	1.05
	L/3	9.66	56.32	LB	LB	8.69	54.55	DB+LB	DB+LB	1.11	1.03
	L/2	8.52	46.41	LTB	DB+LB	8.25	49.17	LTB	DB+LB	1.03	0.94
BBC-10015	L/6	13.75	64.37	LB	LB	15.8	72.77	LB	LB	0.87	0.88
	L/4	13.53	62.66	LB	LB	15.21	72.52	LB	LB	0.89	0.86
	L/3	13.7	65.11	LB	LB	14.53	68.84	DB+LB	DB+LB	0.94	0.95
	L/2	12.88	56.01	LTB	DB+LB	11.69	50.86	LTB	DB+LB	1.10	1.10
BBC-10019	L/6	19.56	67.00	LB	LB	23.00	76.50	LB	LB	0.85	0.88
	L/4	19.60	68.48	LB	LB	21.98	84.05	LB	LB	0.89	0.81
	L/3	19.54	68.04	LB	LB	20.11	62.62	DB+LB	DB+LB	0.97	1.09
	L/2	18.83	64.69	LTB	DB+LB	16.94	54.07	LTB	DB+LB	1.11	1.20
BBC-15012	L/6	15.83	30.38	LB	LB	17.06	32.23	LB	LB	0.93	0.94
	L/4	15.31	30.00	LB	LB	14.3	28.86	LB	LB	1.07	1.04
	L/3	15.82	30.18	DB+LB	DB+LB	16.28	33.23	DB+LB	DB+LB	0.97	0.91
	L/2	12.8	24.96	LTB	DB+LB	14.21	26.22	LTB	DB+LB	0.90	0.95
BBC-15015	L/6	23.51	37.3	LB	LB	22.62	38.52	LB	LB	1.04	0.97
	L/4	22.69	34.07	LB	LB	22.72	38.19	LB	LB	0.99	0.89
	L/3	23.5	37.1	DB+LB	DB+LB	24.98	36.9	DB+LB	DB+LB	0.94	1.01
	L/2	19.93	30.36	LTB	DB+LB	23.22	33.94	LTB	DB+LB	0.86	0.89

Δ : Maximum vertical displacement at the section A-A 100 mm from mid-span; L: representative span length (3.5m); C1: one C section side; C2: another C section side; LB: local buckling; DB: distortional buckle; LTB: lateral torsional buckle; L/6, L/4, L/3, L/2= 583, 875, 1167, 1750mm respectively.

4.2.1 Key factors improving load capacity of the beam

Figure 4.9 shows the maximum load and web height to thickness ratio curve that have been plotted both results from experiment and finite element analysis. From high web height to thickness ratio to low web height to thickness ratio, both from experimental results and finite element analysis results have the same manner. The curve increases significantly with both left and right group. Even the results getting from FEA, it shows that thickness is a very important factor to increase the load capacity of the beam. Moreover, connection spacing decreases the max load to web height to thickness ratio curve also increase both experiment and FEA. The plot of flange width to thickness ratio was demonstrated in Figure 4.10 and the same tendency was confirmed.

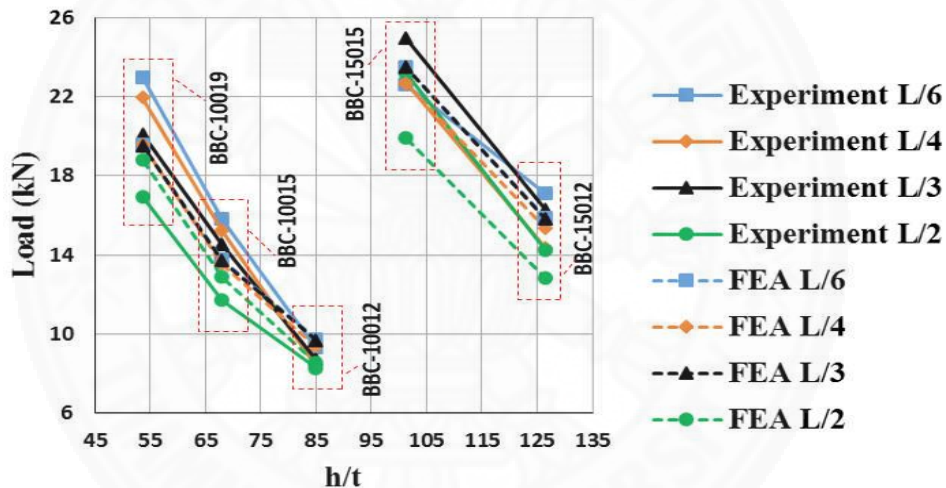


Figure 4.9 Max load-web height to thickness ratio curve of experiment and FEA with L/6, L/4, L/3, and L/2

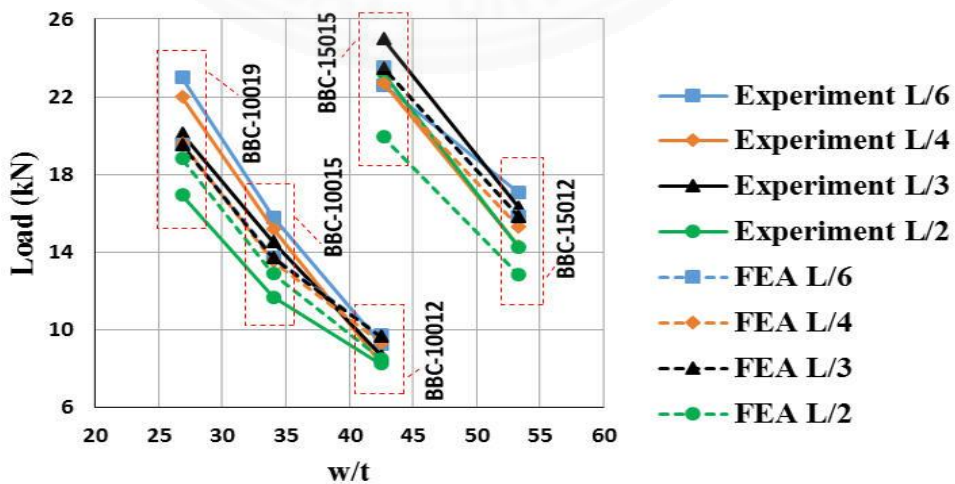


Figure 4.10 Max load-flange width to thickness ratio curve of experiment and FEA with L/6, L/4, L/3, and L/2

4.2.2 Comparison of load-vertical deflection curve between experimental and FEA results

From Figure 4.11 to Figure 4.15 shows the comparison of load-vertical deflection curve between experimental and FEA results of all 20 specimens. FEA curves closely match with the experimental curves, especially the model with the connection spacing $L/3$. However, there are some differences among the FEA and experimental curves. To improve the FEA results, some conditions in the finite element models need to be modified, such as modeling of screw connection.

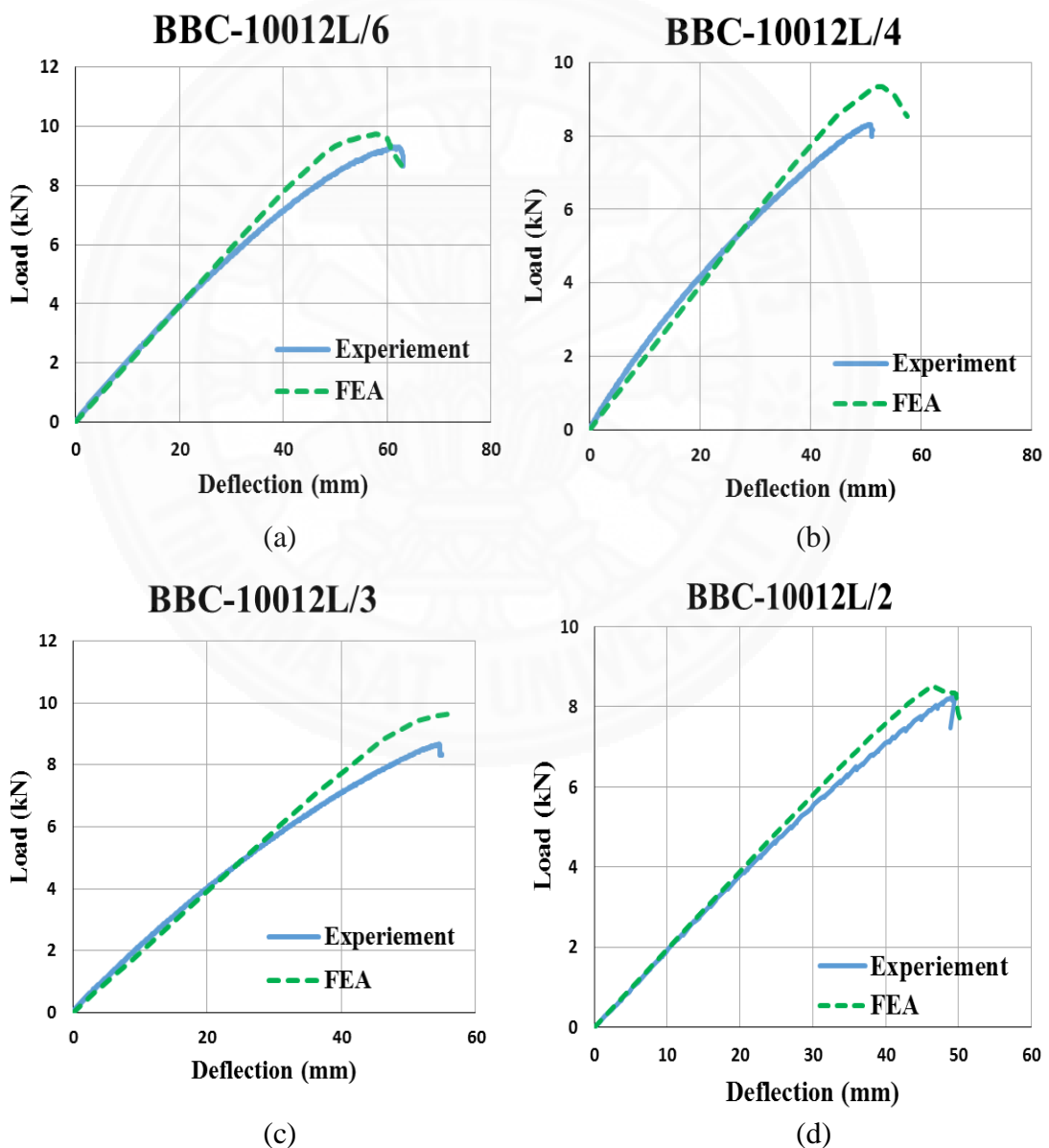


Figure 4.11 Comparison of load-vertical deflection curve between experimental and FEA results: (a): BBC-10012L/6; (b): BBC-10012L/4; (c): BBC-10012L/3; (d): BBC-10012L/2

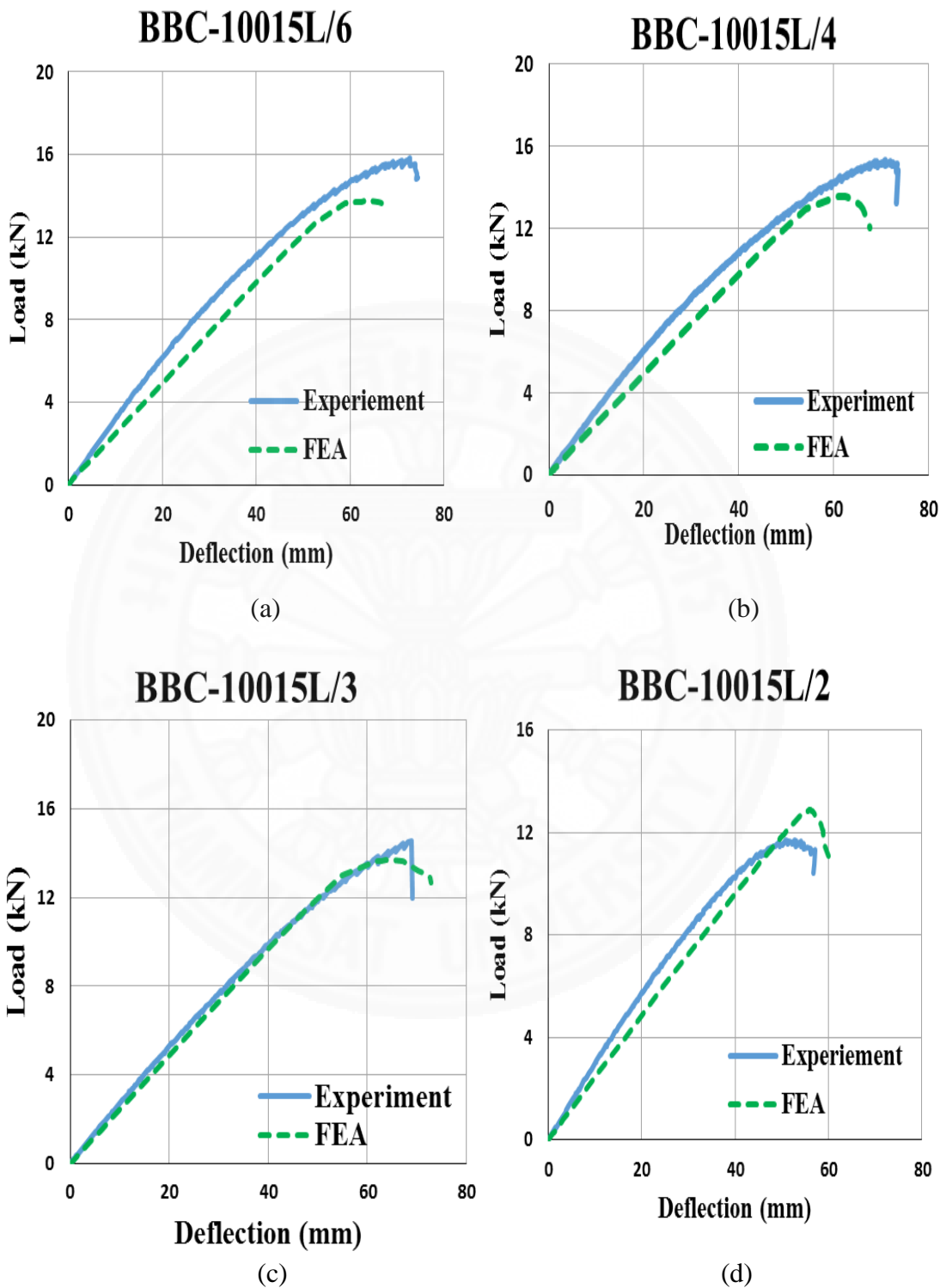


Figure 4.12 Comparison of load–vertical deflection curve between experimental and FEA results: (a): BBC-10015L/6; (b): BBC-10015L/4; (c): BBC-10015L/3; (d): BBC-10015L/2

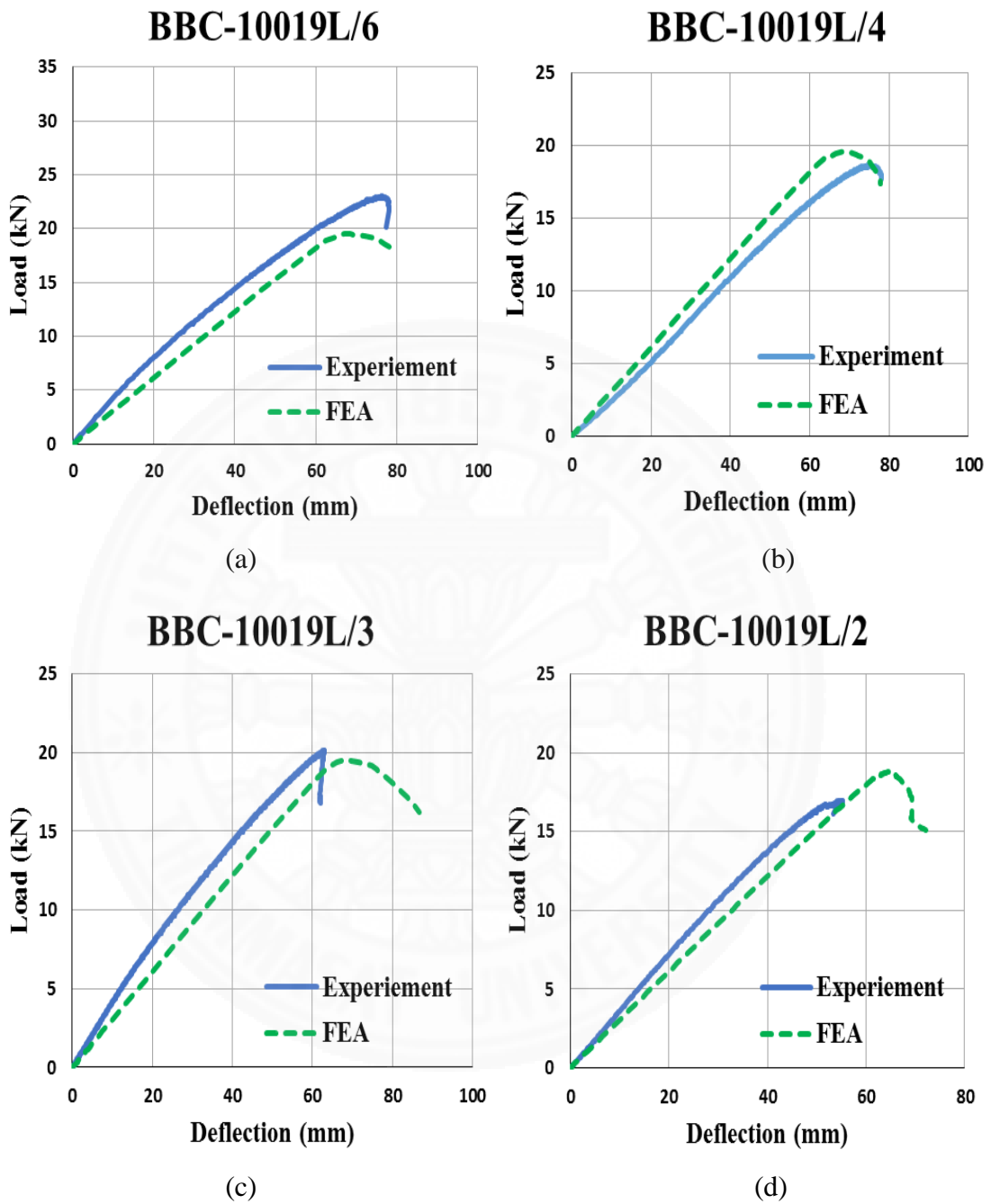


Figure 4.13 Comparison of load–vertical deflection curve between experimental and FEA results: (a): BBC-10019L/6; (b): BBC-10019L/4; (c): BBC-10019L/3; (d): BBC-10019L/2

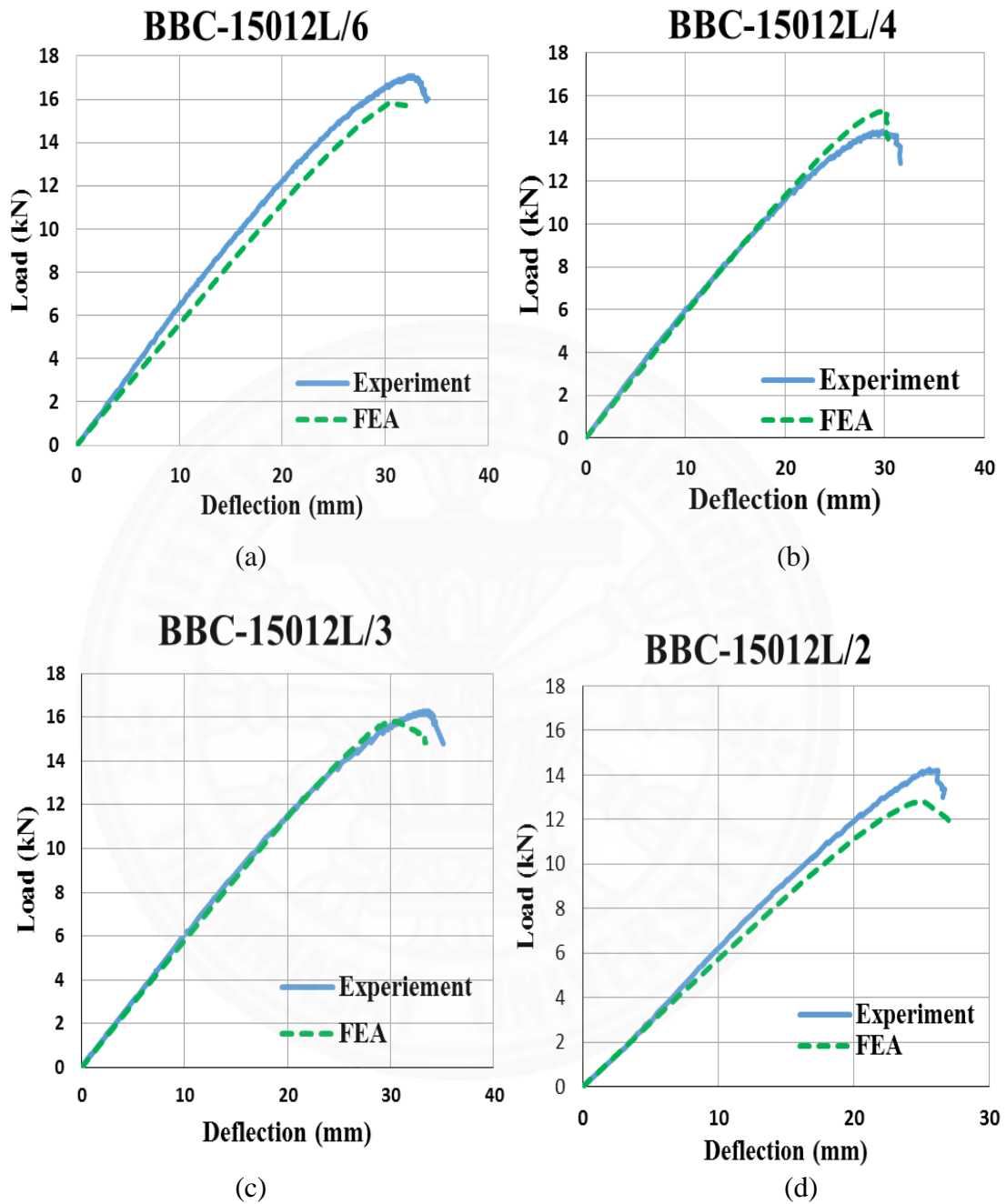


Figure 4.14 Comparison of load–vertical deflection curve between experimental and FEA results: (a): BBC-15012L/6; (b): BBC-15012L/4; (c): BBC-15012L/3; (d): BBC-15012L/2

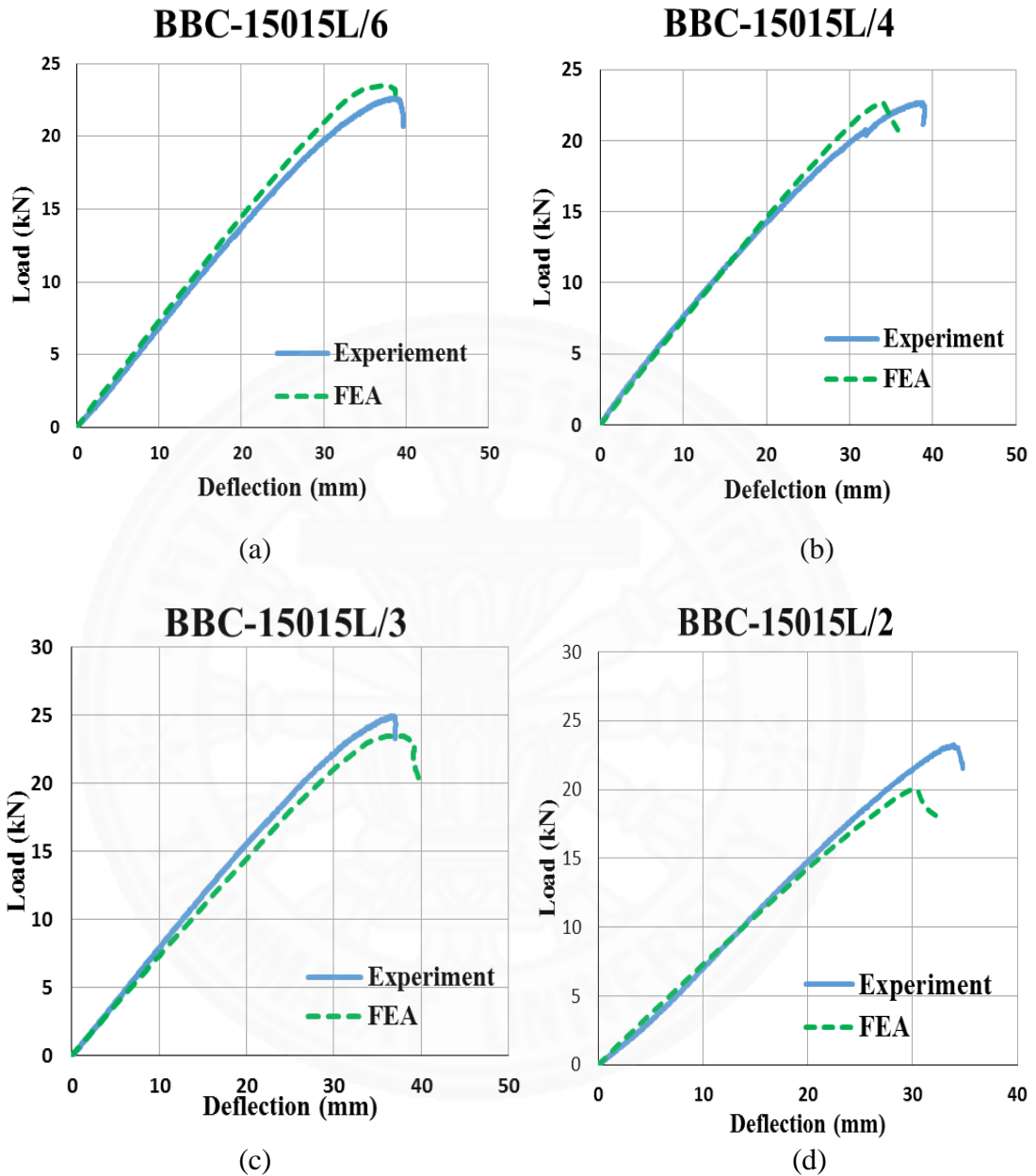
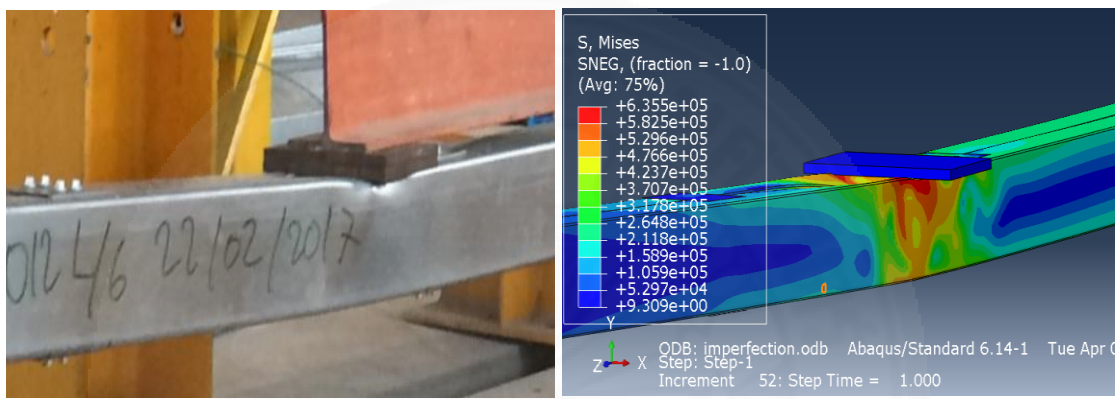


Figure 4.15 Comparison of load–vertical deflection curve between experimental and FEA results: (a): BBC-15015L/6; (b): BBC-15015L/4; (c): BBC-15015L/3; (d): BBC-15015L/2

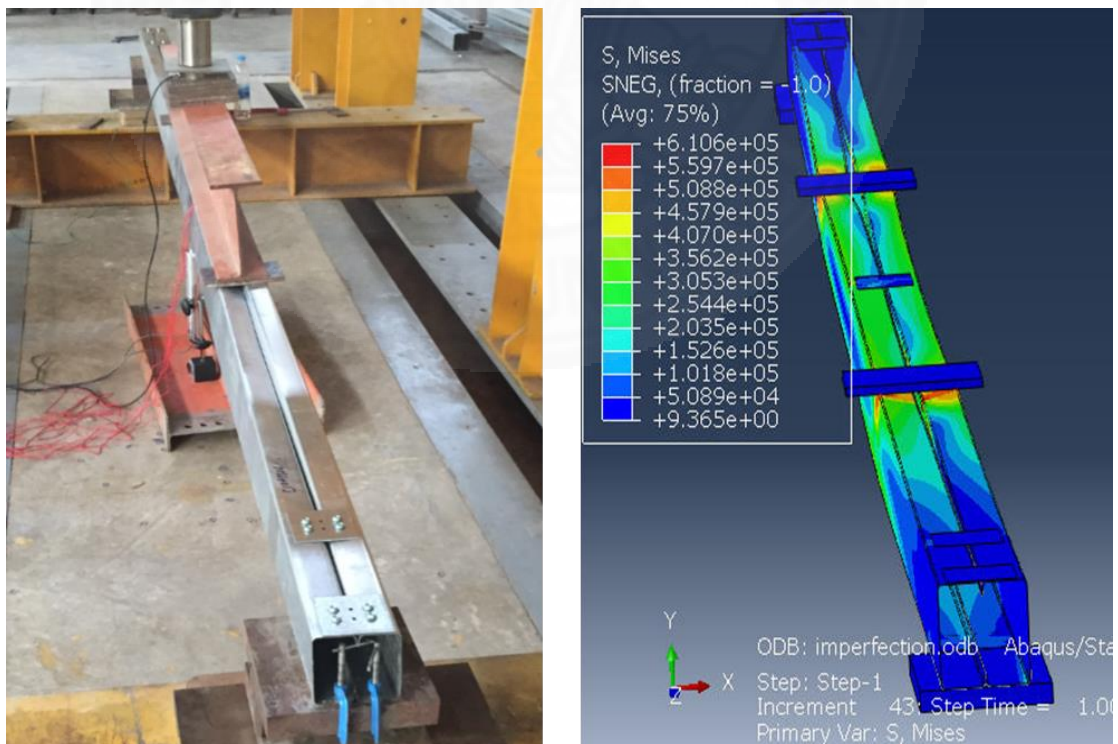
4.2.3 Comparison of failure mode from experiment and FEA

Comparison of failure modes from experiment and finite element analysis have been shown from Figure 4.16 to Figure 4.20. It was found that from both numerical and experimental results, the beam failed in local buckling for all specimens with

connection spacing $L/6$ and $L/4$. In addition, the same failure modes of the beams with connection spacing $L/2$ which are lateral torsional, distortional, and local buckling were observed from both results. There are some differences for the smaller section BBC-10012, BBC-10015, and BBC-10019 in case of connection spacing $L/3$. Distortional buckling has not been found from the finite element analysis results. It showed that the beam have failed in local buckling. However, for the larger section BBC-15012 and BBC-15015, the same failure mode have been reported for both experimental and FEA results.

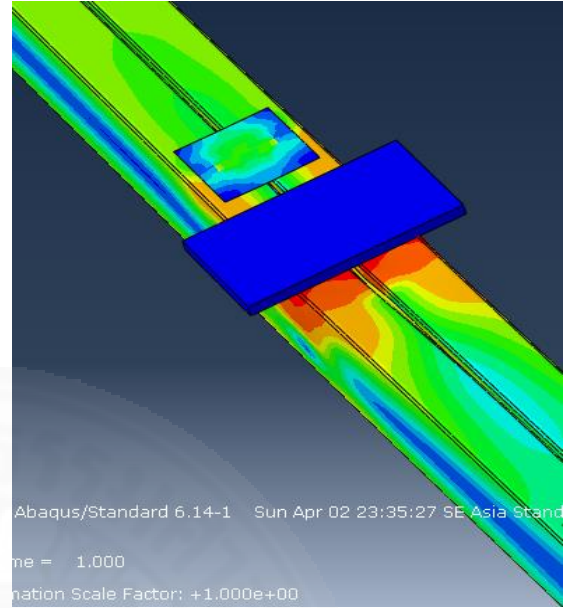


(a): C10012L/6

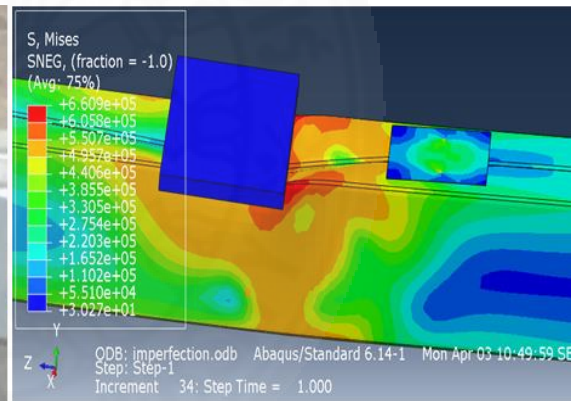


(b): C10012L/2

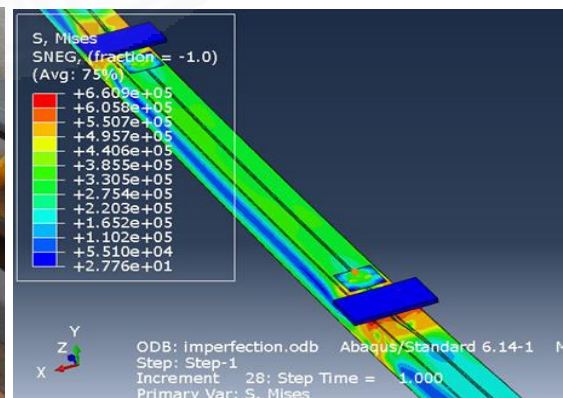
Figure 4.16 Comparison of failure mode from experiment and finite element analysis:
(a): BBC-10012L/6, (b) BBC-10012L/2



(a): C10015L/6

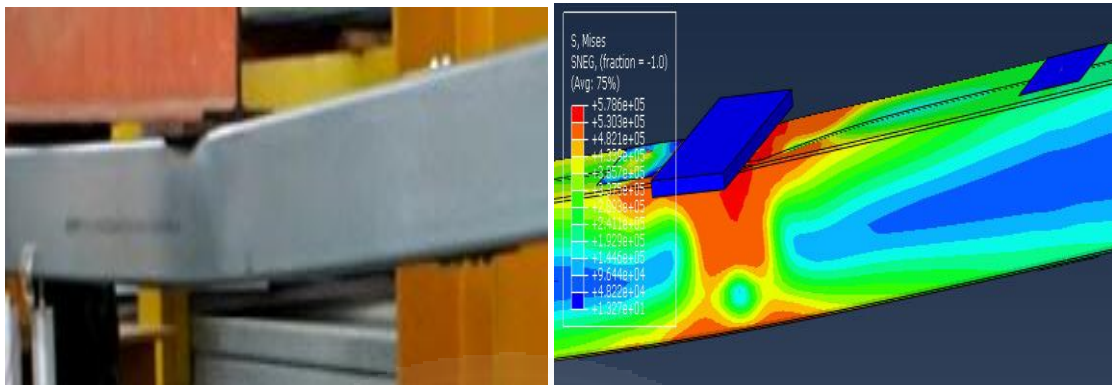


(b): C10015L/4



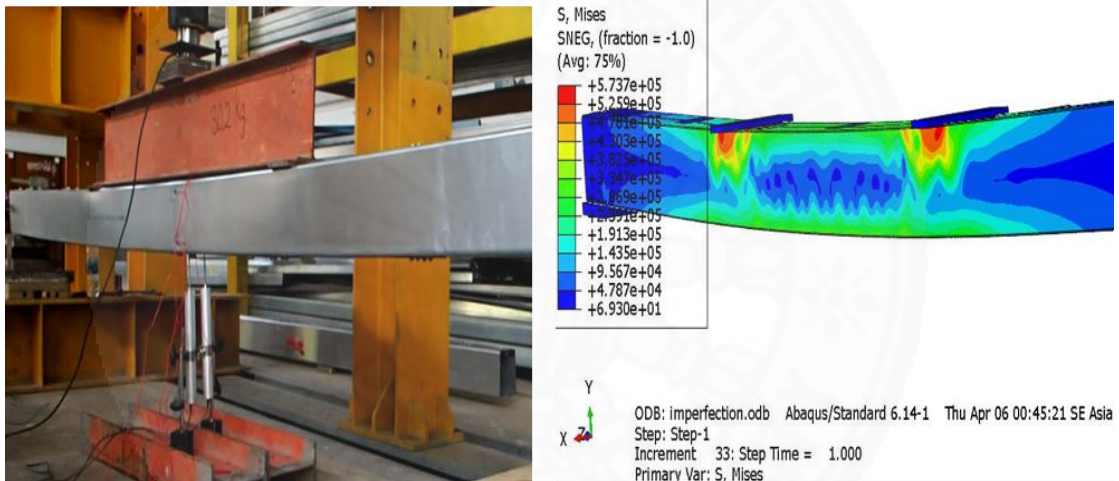
(c): C10015L/3

Figure 4.17 Comparison of failure mode from experiment and finite element analysis:
(a): BBC-10015L/6, (b) BBC-10015L/4, (c) BBC-10015L/3

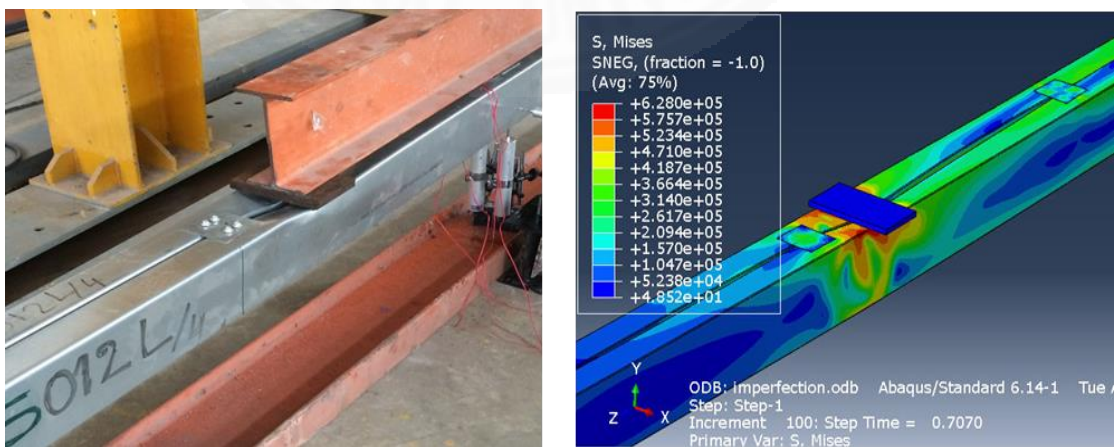


(a): C10019L/6

Figure 4.18 Comparison of failure mode from experiment and finite element analysis:
(a): BBC-10019L/6

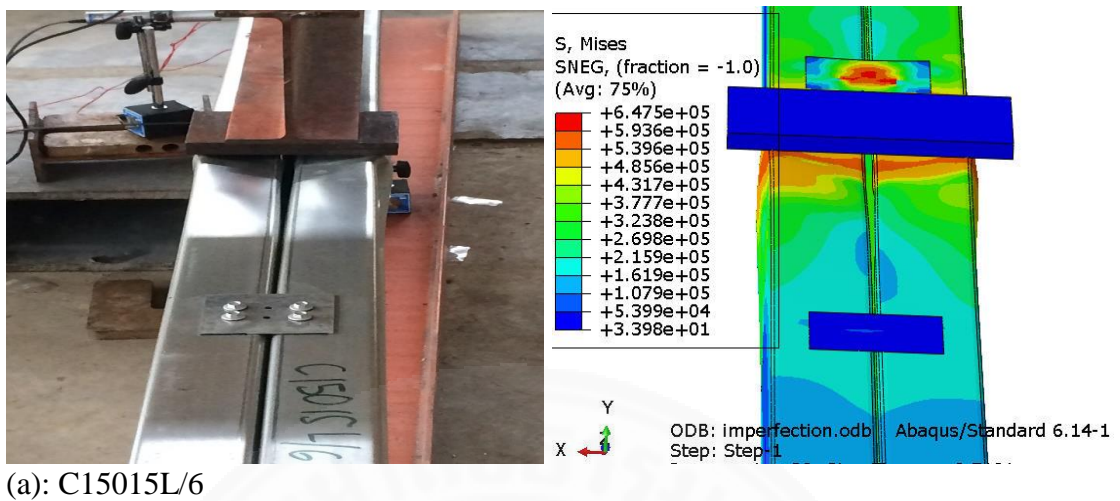


(a): C15012L/6

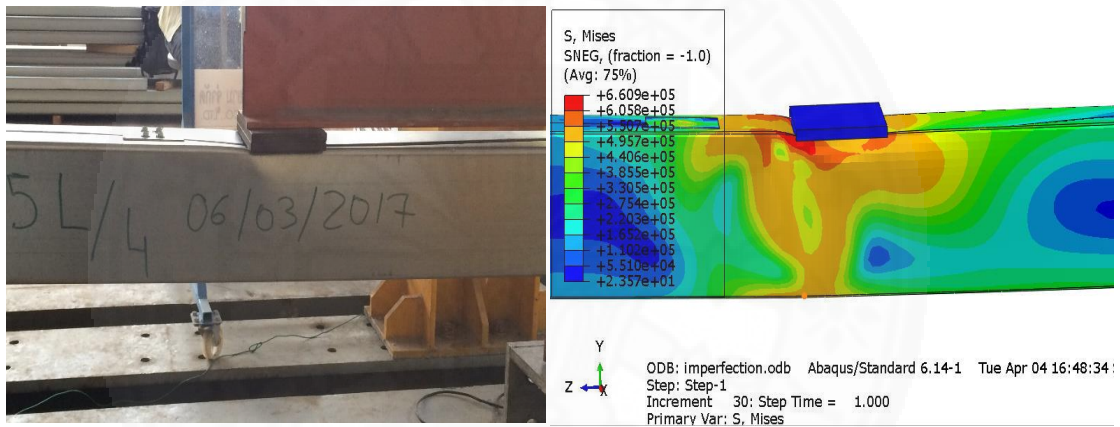


(b): C15012L/4

Figure 4.19 Comparison of failure mode from experiment and finite element analysis:
(a): BBC-15012L/6, (b) BBC-15012L/4



(a): C15015L/6



(b): C15015L/4

Figure 4.20 Comparison of failure mode from experiment and finite element analysis:
(a): BBC-15015L/6, (b) BBC-15015L/4

Chapter 5

Conclusion and Recommendation

Behavior of cold-formed steel built-up box beam that consists of two C sections having stiffening plate with self-drilling screws has been investigated in this research. A series of flexural test on the twenty box beam specimens have been performed. Built-up box beams made of five different C sections: C10012, C10015, C10019, C15012, and C15015 were tested. The total length of the beam specimen is 4 meters. In addition, four different connection spacings equal to $L/2$, $L/3$, $L/4$, and $L/6$ (where $L = 3.5$ m is representative span length) were chosen. Moreover, the dimension of the connection plate is $80 \times 80 \times 2$ mm and the radius of the screw is 1.95 mm. Finite element models were established to simulate buckling failure and investigate the load capacity in order to validate with the experimental results. Geometric nonlinearity, material nonlinearity, and initial geometric imperfections were considered in the finite element analysis. From the results of experiment and FEA, the following conclusion can be drawn:

1. Experimental results show that the load capacity of the beam increases when the thickness increases and the connection spacing decreases. In case of the same web height, web height to thickness ratio increases, the load capacity of the beam drops dramatically. For flange width to thickness ratio, in case of the same flange width, the same tendency is confirmed.
2. Comparing load capacity of the $L/2$ and $L/6$ beam, maximum load can increase in range up to 35.77% of $L/2$ beam. In addition, increasing thickness from 1.2 to 1.5 mm for BBC-100, maximum load of the beam increases 41.73% to 82.79%. For 1.5 to 1.9 mm for BBC-100, it increases from 38.35% to 45.55%. Moreover, changing thickness from 1.2 to 1.5 for BBC-150, ultimate load get higher in the range of 32.60% to 63.41%.
3. From the experimental results, the failure modes with connection spacing $L/4$ or smaller were local buckling, and the failure modes with connection spacing larger than $L/4$ were mixed modes of local buckling and distortional buckling, or lateral torsional buckling. For the design recommendation, the connection

spacing to form the built-up box beam should be the connection spacing $L/4$ or smaller.

4. It can be seen that the difference between ultimate load from FEA and the experiment was between -15% and +12% and the difference between vertical displacement at failure from FEA and the experiment was between -19% and +20%.
5. For larger section like BBC-15012 and BBC-15015, the failure modes from numerical analysis and the test have found to be the same with all kinds of connection spacing. However, failure modes between FEA and the test of smaller sections BBC-10012, BBC-10015, and BBC-10019 in case of connection spacing $L/6$, $L/4$, and $L/2$ were similar. On the other hand, for these smaller sections in case of connection spacing $L/3$, FEA results showed that the beams failed in local buckling. In contrast, from the test results, the failure mode was distortional and local buckling.

For further study, it was recommended that improving or changing some conditions in finite element model is needed in order to obtain more accurate results and to understand more deeply. 3D element of screw to represent its realistic is appreciably encouraged. In addition, larger sections should be investigated. Another recommendation is varying the span length for further study and the influence of height to span length ratio should be investigated in order to propose the design method for built-up box section beam that will be very useful in the future.

References

- AISI, North American Specification for the Design of Cold-Formed Steel Structural Members, S100-12, ed., 2012.
- B. W. Schafer, Z. Li, and C. D. Moen (2010) "Computational modeling of Cold-formed steel", *Journal of Thin-Walled Structures* 48, pp. 752-762.
- D. Dubina, V. Ungureanu, and R. Landolfo (2012). *Design of cold-formed steel structures*. Portugal: ECCS – European Convention for Constructional Steelwork
- G. J. Hancock (2003) "Cold-formed Steel Structures", *Journal of Constructional Steel Research* 59, pp. 473-487.
- H. T. Tran, W. Patwichaichote, and T. Chaisomphob (2015) Experimental study on flexural behavior of cold-formed steel built-up c section beam. *Proceeding of the 9th Asia Pacific Structural Engineering and Construction Conference (APSEC 2015) and 8th Asean Civil engineering Conference (ACEC 2015)*, Kuala Lumpur, Malaysia, pp. 79-84.
- H. T. Tran, W. Patwichaichote, T. Chaisomphob, and E. Yamaguchi (2016) Numerical study on flexural behavior of cold-formed steel built-up c section beam. *Proceeding of The 14th East Asia-Pacific Conference on Structural Engineering and Construction (EASEC-14)*, Ho Chi Minh City, Vietnam, pp. 1855-1861.
- I. Faridmehr, M. Md. Tahir, M. H. Osman, A. F. Nejad, and R. Hodjati (2015) "An experimental investigation of stiffened cold-formed C-channels in pure bending and primarily shear conditions". *Journal of Thin-Walled Structures* 96, pp. 39-48.
- L. Xu, P. Sultana, and X. Zhou (2009) "Flexural strength of coldformed steel built up box sections". *Journal of Thin-Walled Structures* 47, pp. 807-815.
- L. Laím, J. P. C. Rodrigues, and L. S. da Silva (2013) "Experimental and numerical analysis on the structural behavior of cold formed steel beams". *Journal of Thin-Walled Structures* 72, pp. 1-13.

- L. Laim. *Experimental and Numerical analysis on the structural behavior of cold-formed steel beams subjected to fire*. Thesis (PhD), University of Coimbra, Portugal, 2013.
- L. Wang, and B. Young (2016) “Behavior of Cold-formed Steel Built-up Sections with Intermediate Stiffeners under Bending. II: Parametric Study and Design”, *Journal of Structural Engineer* 142(3), 04015151, pp. 1-11.
- N. S. Trahair (1993). *Flexural-torsional buckling of structures*. London: CRC Press.
- P. Manikandan, and S. Sukumar (2016) “Behaviour of cold-formed steel built-up closed section with intermediate web stiffener under bending”, *Asian Journal of Civil Engineering (BHRC)*, Vol. 17, No. 2, pp. 249-257.
- P. Sultana. *Predictions of Flexural Behaviour of Built-up Cold-formed Steel Sections*. Thesis (Master), University of Waterloo, Waterloo, Canada, 2007.
- Simulia. (2010). *Abaqus 6.10/Analysis User's Manual, Volume II: Analysis*. RI, USA: Dassault Systemes.
- “Simulia. ABAQUS/CAE. Version 6.14-1”, Available: <http://abaqus.software.polimi.it/v6.14/books/usi/default.htm> [Accessed: Apr, 2017]
- V. Raghul, and N. U. Maheswari (2015) “Analytical Investigation On Cold-formed Steel Built-up Section Under Flexure”, *International of Advanced Engineering Research and Technology (IAERT)*, Volume 4, Issue 4, pp. 108-114.
- Y. L. Li, Y. Q. Li, and Z. Y. Shen (2016) “Investigation on flexural strength of cold-formed thin-walled steel beams with built-up box section”, *Journal of Thin-Walled Structures* 107, pp. 66-79.